

Draft
Pending
technical review

PAVEMENT SUBGRADE PERFORMANCE STUDY

Accelerated pavement testing of A-2-4 subgrade soil
at wetter than optimum moisture content

VINCENT JANOO AND EDEL CORTEZ

U.S. Army Cold Regions Research and Engineering Laboratory
72 Lyme Road
Hanover, New Hampshire 03755, United States

Subgrade Moisture Content	AASHTO Soil Type			
	A-2-4	A-4	A-6	A-7-6
M1	Optimum 10% TS 701	Optimum 17% TS 702	Optimum 16%	Optimum TBD*
M2	12% TS 707	19% TS 704	19% TS 708	TBD
M3	15% TS 703	23% TS 705	22% TS 706	TBD

EXECUTIVE SUMMARY

This is the seventh in a series of reports on the pavement subgrade failure criteria research study conducted in the Frost Effects Research Facility (FERF) at the U.S. Army Corps of Engineers, Engineer Research and Development Center, Cold Regions Research and Engineering Laboratory in Hanover, New Hampshire. The hypothesis for the study is that the pavement failure criterion depends on the subgrade type and the in-situ moisture content. Many of the current mechanistic design procedures incorporate the results from AASHTO Road Tests conducted in the late fifties. The criterion is based on one soil type (A-6), and, most of all, it was difficult to discern the effect of load and environment on the failure criterion. Our assertion is that the criterion is not applicable to other subgrades and possibly to areas other than where it was developed. Also, the criterion was inferred from surface distresses rather than from actual in-situ stress and/or strain measurements.

As part of the research program, four subgrade soils were selected for testing in the FERF. The test program includes testing each subgrade soil at three moisture contents. One of the subgrade moisture conditions was designed to be at or near optimum density and moisture content. A second moisture condition was designed to be at higher than optimum moisture content, and a third moisture condition was designed to be at lower than optimum moisture content. A test section was built or will be built to represent each soil at each of the three moisture conditions.

The test sections, consisting of 76 mm of asphalt concrete and 203 mm of crushed base over the test subgrade soil, were instrumented with stress, strain, moisture, and temperature sensors. The test sections were then subjected to accelerated loading under controlled environmental conditions.

This report presents the results from the accelerated pavement for one of the test subgrade soils. The subgrade, based on AASHTO soil classification system, was an A-2-4. It was constructed at a density and moisture content of 1930 kg/m³ and 12% by weight, respectively, which is wetter than optimum. During construction the layer density and moisture content were recorded. Accelerated traffic load testing was applied to each of six test windows in this test section. Each test window was approximately 6.0 m long and 1 m wide. Traffic loads were applied uni-directionally at an average speed of 12 km/hr. All six windows were tested, and the loads varied between 40 and 80 kN. The load was applied through dual truck tires, with the tire pressures averaging around 690 kPa.

Stress, strain, and surface rut measurements were taken periodically in all of the windows. All stress measurements were taken in the subgrade at

approximately 381 mm from the top of the subgrade. In two of the test windows, stress measurements were also taken at 686 mm from the top of the subgrade. Dynamic and permanent strains in the base and subgrade were measured in all windows.

This report presents the measured response of this test section to accelerated loading. The results showed that the effect of increasing the moisture content decreased the limiting strain. The limiting strains are significantly different from the strains predicted from either the current Asphalt Institute and Shell subgrade failure criteria. The current criterion is inadequate for an A-2-4 subgrade soil with high moisture contents. The Asphalt Institute criterion underestimates the limiting strains by about 20–50%, with the difference getting smaller as the load repetition increases. For the Shell criterion, the difference is about 40–50%.

CONTENTS

EXECUTIVE SUMMARY	ii
1 INTRODUCTION.....	1
2 MATERIAL PROPERTIES OF THE SOIL	2
3 CONSTRUCTION OF THE TEST SECTION.....	4
Construction Control.....	5
Instrumentation.....	6
4 TESTING PROGRAM.....	11
Accelerated Loading of the Test Sections	12
Back-calculation of FWD Data	13
Surface Rut Measurements.....	16
Strain Measurements	19
Stress Measurements	23
5 FORENSICS	27
Forensic Testing	27
Forensic Observations.....	39
6 SUMMARY AND CONCLUSIONS.....	40
REFERENCES	42

ILLUSTRATIONS

Figure 1. Grain size distribution of the subgrade and base course materials	2
Figure 2. Plan and cross sectional views of Test Section 707	4
Figure 3. Distribution of densities in the test subgrade	5
Figure 4. Distribution of moisture content in the test subgrade	6
Figure 5. Location of FWD test points in TS 707	11
Figure 6. Location of test wheels over coil and stress cells	12
Figure 7. Impulse Stiffness Modulus at FWD test locations	14
Figure 8. Longitudinal rut formation as a function of load repetitions	17
Figure 9. Rut depth progression as a function of load repetitions	18
Figure 10. Permanent deformations of the top of the subgrade layer	19
Figure 11. Development of permanent strains on the top of the subgrade as a function of load repetitions	20
Figure 12. Permanent deformations at failure on the top of the subgrade	21

Figure 13. Peak dynamic vertical displacements at the top of the subgrade as a function of load repetitions	22
Figure 14. Peak dynamic vertical strains of the subgrade as a function of load repetitions	22
Figure 15. Comparison of calculated and measured stresses	26
Figure 16. Subgrade mean gravimetric moisture content from the time of construction to the time of the forensic evaluation	27
Figure 17. Location of the forensic trenches in TS 707	28
Figure 18. Dry saw cutting of the asphalt layer	28
Figure 19. Thickness measurements in the asphalt concrete layer and in the base course in cross sections of the six test windows	29
Figure 20. Nuclear gage density measurements in the trenches	32
Figure 21. Gravimetric moisture content in the two forensic trenches obtained with a nuclear gage	33
Figure 22. Soil dry density in the two forensic trenches obtained with a nuclear gage	34
Figure 23. Soil dry density in the two forensic trenches obtained with a sand cone	35
Figure 24. Portable falling weight deflectometer being used in the trenches	36
Figure 25. Soil modulus as measured with the portable falling weight deflectometer in the two forensic trenches	36
Figure 26. Dynamic cone penetrometer	38
Figure 27. CBR values obtained from DCP measurements in the two forensic trenches	38
Figure 28. Effect of soil type on the subgrade failure criterion	41

TABLES

Table 1. TS707 subgrade soil properties	3
Table 2. Locations of the emu coils in the test windows	7
Table 3. Depths of pressure sensors in the test section	8
Table 4. Mean volumetric moisture content for the nine sensors in the test section during accelerated pavement testing	9
Table 5. Mean subsurface temperatures in the test section during accelerated pavement testing	10
Table 6. Mean tire loads for each test window	12
Table 7. Deflections normalized to 40 kN	13
Table 8. Pavement layer thicknesses used in the back-calculation process	14
Table 9. Initial and seed moduli used for the various layers	15
Table 10. Back-calculated layer moduli (WESDEF)	15

Table 11. Back-calculated layer moduli with a fixed AC modulus (WESDEF)	16
Table 12. Back-calculated layer moduli (ELMOD5)	16
Table 13. Load repetitions to reach a failure of 12.5 mm	19
Table 14. Power curve coefficients for the vertical permanent strains	20
Table 15. Power curve coefficients for the vertical strains	23
Table 16. Peak stresses in the top of the subgrade under applied load	23

PAVEMENT SUBGRADE PERFORMANCE STUDY

Accelerated Pavement Testing of A-2-4 Subgrade Soil at Wetter than Optimum Moisture Content

VINCENT JANOO AND EDEL CORTEZ

1 INTRODUCTION

This is Volume 7 in a series of reports containing details and results from Test Section 707. TS 707 was constructed in the Frost Effects Research Facility (FERF) at the Engineer Research and Development Center, Cold Regions Research and Engineering laboratory (ERDC/CRREL) in Hanover, New Hampshire. A detailed description of the FERG can be found in Janoo et al. (2002).

TS 707 was built with a test subgrade classified as an A-2-4 according to the AASHTO soil classification system and was constructed at a density and moisture content of 1930 kg/m³ and 12%, respectively. The pavement structure consisted of 76 mm of asphalt concrete (AC) over a 229-mm crushed aggregate base over 2.75 m of test subgrade.

The test section was again divided into six test windows, and each window was subjected to accelerated loading using the Heavy Vehicle Simulator (HVS).

Surface rut depth measurements were taken periodically during the accelerated load tests. Failure was assumed to occur when the surface rut depth equaled or exceeded 12.5 mm. The test windows were instrumented with stress and deformation sensors. In addition, temperature and moisture sensors were installed at various depths in the test section. Subsurface stress and strain measurements were recorded periodically, whereas subsurface moisture and temperatures were recorded hourly.

2 MATERIAL PROPERTIES OF THE SOIL

The subgrade soil was a blend of an A-1 soil obtained from a local quarry and an A-4 soil to produce the A-2-4 (AASHTO classification) or SM (ASTM) soil (Fig. 1). Routine classification tests conducted on the test soil included optimum moisture, maximum density, gradation and hydrometer analyses, specific gravity, and liquid and plastic limits. Standard AASHTO test procedures were used. The A-2-4 subgrade soil has approximately 30% passing the 0.074-mm sieve. The average liquid limit (LL) and plasticity index (PI) of the soil were 30% and 2.1, respectively. The average specific gravity was 2.72. The average optimum density and moisture content (AASHTO T 99-90) were 1934 kg/cm³ and 10%, respectively. The results from the classification tests are summarized in Table 1.

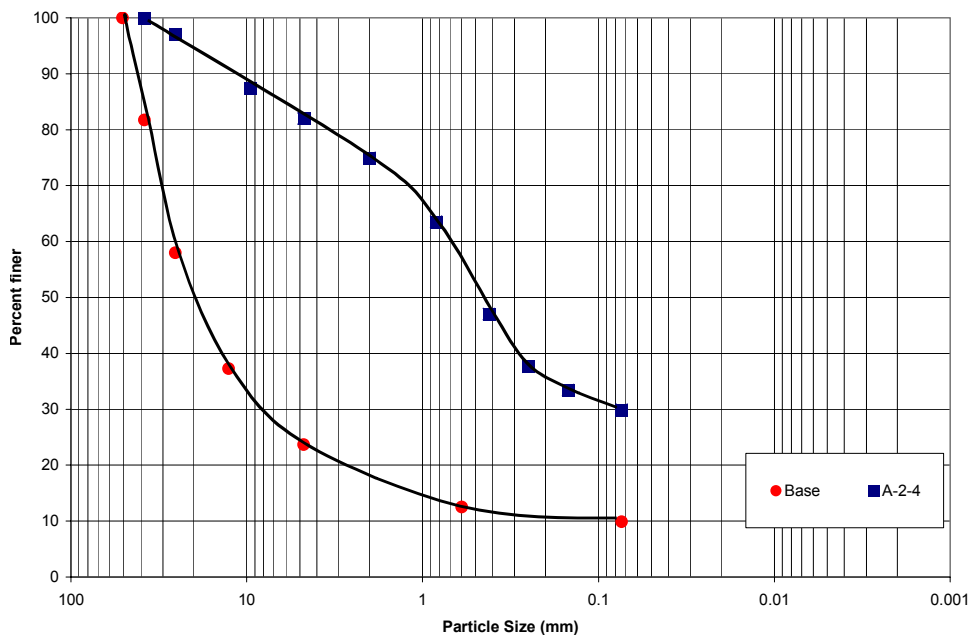


Figure 1. Grain size distribution of the subgrade and base course materials.

The base course was crushed gravel classified as No. 304 under NH State DOT base course specification, equivalent to an AASHTO A-1-a or ASTM GP-GM. The gradation of the base course is shown in Figure 1. The asphalt material of the binder course conformed to the Vermont Type II standard, with 19-mm maximum aggregate particle size and 4.5% of asphalt binder PG-58-34. The asphalt concrete material of the wearing course conformed to the Vermont Type

III standard, with 13-mm maximum aggregate particle size and 5.3% of asphalt binder PG-58-34. The nominal thickness of the binder course was 51 mm. The nominal thickness of the wearing course was 25 mm.

Table 1. TS707 subgrade soil properties.

Soil type	AASHTO A-2-4
Specific gravity	2.72
Liquid limit	30
Plasticity index	2.1
Pass #10 sieve	71.8%
Pass #200 seive	29.9%
Optimum moisture content	10%
As-built moisture content	12%
Optimum density	1934 kg/m ³
As-built average density	1930 kg/m ³

3 CONSTRUCTION OF THE TEST SECTION

The available area for the test section was 42 m long by 6.4 m wide and 3.7 m deep. The actual length used for testing was approximately 23 m long (Fig. 2). As shown in Figure 2, there are the six test windows (designated C1–C6) within the test area for conducting accelerated load tests. Each test window was 7.8 m long, of which the beginning and the end 0.9 m were used as acceleration and deceleration areas for the wheel. The area in between the ends (6 m long by 0.9 m) was where the constant velocity tests were conducted. The center-to-center distance between the test windows was 1.2 m.

The cross section of TS 707 consisted of a nominal 76-mm layer of asphalt concrete over a nominal 229-mm crushed base course over the test subgrade. The specifications required that the subgrade be constructed in 150-mm-thick lifts and that each lift be compacted at moisture contents within $\pm 2\%$ of the optimum and to a density between 95 and 100% of the maximum dry density obtained from the Standard AASHTO T99 test procedure. The A-2-4 subgrade soil was preconditioned for a target moisture content of $12\% \pm 2\%$. The optimum moisture content for this soil was 10%.

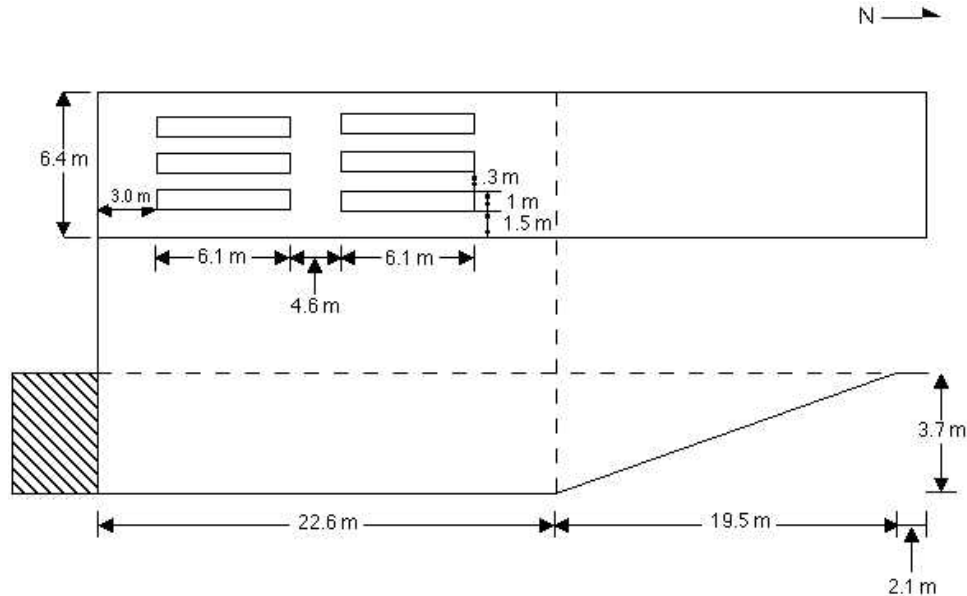


Figure 2. Plan and cross sectional views of Test Section 707.

Construction Control

During the construction of the subgrade, a series of tests were conducted on the compacted layers. These measurements were conducted on every 300-mm lift unless otherwise noted. Measurements included layer thickness, which were taken with a survey level, and in-place Troxler nuclear moisture/density measurements. A total of 360 measurements were taken in the subgrade layer and 42 measurements in the base and AC layers. Density measurements for the AC layer were taken after the accelerated pavement testing. Other measurements included elevation measurements on top of the subgrade, base and AC layers and falling weight deflectometer (FWD) tests on top of the completed test section.

The mean dry density of the subgrade was 1930 kg/m³ with a COV of 2.5% (Fig. 3). For the base the mean density was 2162 kg/m³ with a COV of 5.5%. The mean density of the AC was 2284 kg/m³ with a COV of 2%. The mean moisture content of the test subgrade was 12% with a COV of 7.5% (Fig. 4). The mean moisture content of the base course was 3.6% with a COV of 12.5%.

The mean subgrade thickness was 3.53 m with a COV of 0.2%. The mean base thickness was 226 mm with a COV of 4%. The mean AC thickness was 71 mm with a COV of 11%.

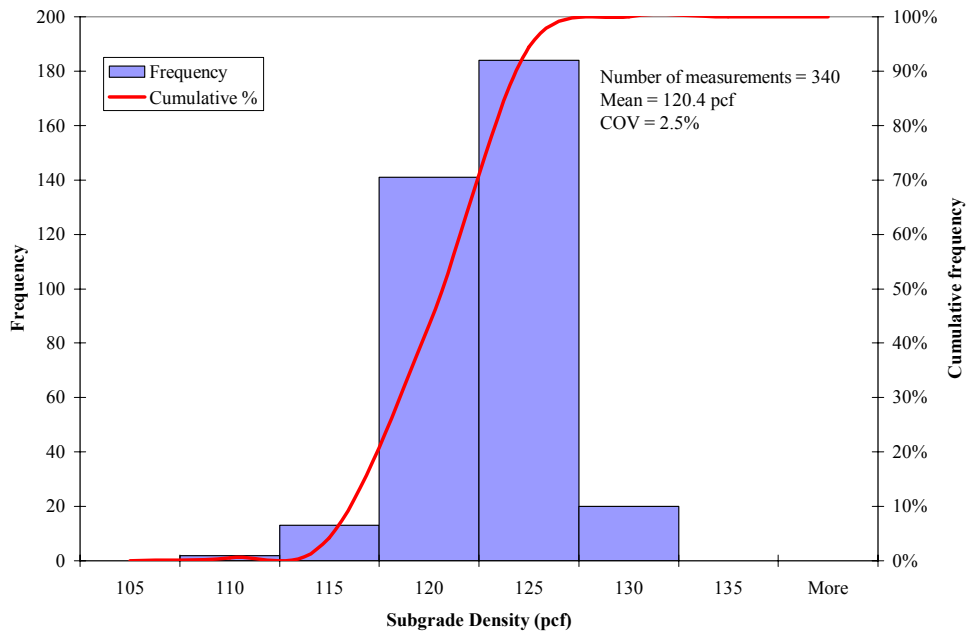


Figure 3. Distribution of densities in the test subgrade.

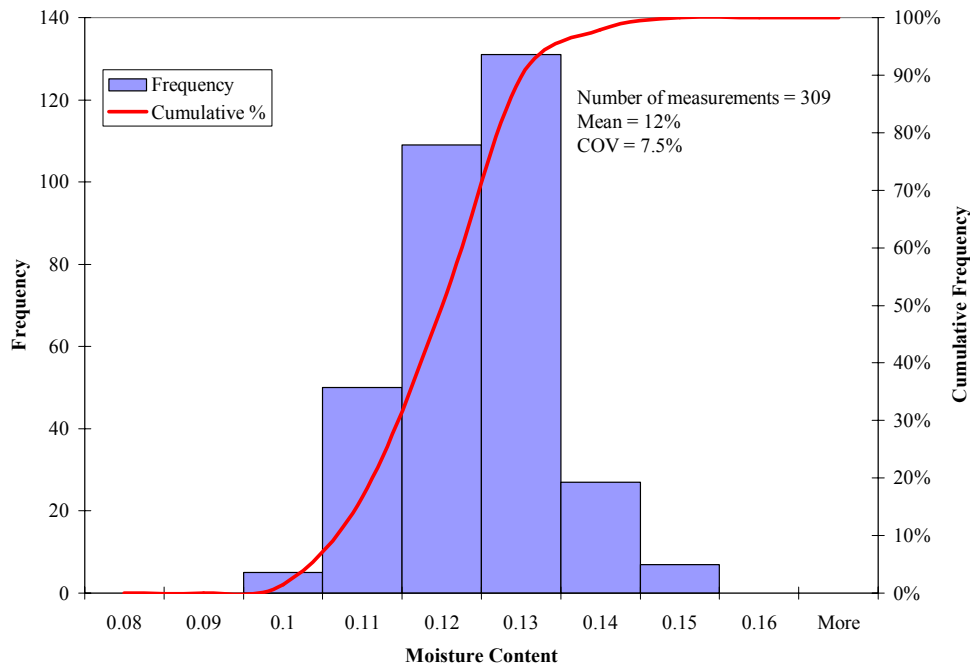


Figure 4. Distribution of moisture content in the test subgrade.

Instrumentation

Instrumentation for measuring stress, strain, temperature, and moisture content was installed in the pavement structure during construction of the test section. Pressures were measured tri-axially in the subgrade using Dynatest pressure cells. In the base course, pressures were measured with Geokon pressure cells. Dynamic and permanent deformations in the base and subgrade were measured with the ϵ mu strain selection. A brief description of the various sensors is provided in this report. A detailed description of the various sensors can be found in Janoo et al. (2002).

Strain Measurements

Triaxial strain measurements were made with the ϵ mu system. The system consists of one sending coil and three receiving coils [longitudinal (x), transverse (y), and vertical (z)], the ϵ mu signal conditioner, and a computer data acquisition system. Details of the system can be found in Janoo et al. (2002). In principle, the system works by passing an alternating current through a coil of wire, generating an alternating magnetic field. Another coil placed within this field will have an alternating current induced in it. The magnitude of the induced current is proportional to the distance between the coils.

Coil sensors were installed in each test window in the base course and subgrade. Their locations as a function of depth are presented in Table 2. They measure the displacements in the vertical direction (designated as the z-direction) and in two perpendicular horizontal directions (x- and y-directions). The z-direction coils are coaxial, while the x- and y-direction coils are coplanar. The x-direction is parallel to the wheel travel, and the y-direction is perpendicular to it.

The coils were installed at eleven depths in columnar stacks, starting below the pavement surface and extending to 1.5 m at a nominal center-to-center spacing of 150 mm in the subgrade. In the base course the nominal distance was 114 mm. Additional sets of coil pairs were installed in TS 707C2 and TS 707C5, starting at a depth of 76 mm and ending at a depth of 610 mm. A loose coil was used on the asphalt surface to measure the permanent deformation of the asphalt layer.

The coil gages were installed after a lift of 300 mm of subgrade soil had been compacted to the desired density and moisture content. A hole approximately 300 mm in diameter was dug to the bottom of the lift (150 mm). The material from the hole was saved in buckets and sealed to ensure that the moisture content did not change. Three coil gages were then installed in the triaxial configuration at the bottom of the hole. Then the saved material was used to fill the hole, which kept the density and moisture content the same as the surrounding material. To ensure that the coil was aligned coaxially with the coil immediately below, the next lower coil was excited and the static response from the upper coil was measured. The coils were aligned when a maximum output from the coil pair was achieved. Once the complete base course was constructed, a hole approximately 300 mm wide and 114 mm deep was dug into the base course layer. Again the dug material was saved in sealed containers. The coil gages were installed and the saved material restored in the hole. Upon final grading of the base course, the top coil pairs were installed just below the surface of the base course.

Stress Measurements

Stress measurements in the base and subgrade were made with Dynatest and Geokon soil pressure cells. Details about these gages can be found in Janoo et al. (2002).

Table 2. Locations of the ϵ mu coils in the test windows.

Gage	Depth (mm)
Coil 1	76
Coil 2	191
Coil 3	305
Coil 4	457
Coil 5	610
Coil 6	762
Coil 7	914
Coil 8	1067
Coil 9	1219
Coil 10	1372
Coil 11	1524

Each test window had three Dynatest pressure cells at a depth of 381 mm from the AC surface. In TS 707C2 and TS 707C5, three additional pressure cells were installed at a depth of 686 mm from the AC surface. In the subgrade the Dynatest pressure cells were orientated to measure the vertical, longitudinal, and transverse stresses. The longitudinal pressure cell was aligned such that the sensing face was in the direction of traffic and was located approximately 305 mm from the vertical pressure sensor. Similarly the transverse pressure sensor was located with the sensing face transverse to the direction of traffic and was located approximately 305 mm from the vertical pressure sensor. Unless otherwise noted, Dynatest stress cells with a range of 10–200 kPa were used to measure the horizontal stresses, while stress cells with a range of 100–800 kPa were used to measure the vertical stresses.

Geokon pressure cells with a diameter of 102 mm were installed in the base course in TS 707C2 and TS 707C5, with the center of the sensing face at a depth of 191 mm from the AC surface to measure the vertical and horizontal stresses from the moving load on the surface. In 707 TSC6 the Geokon pressure cells were installed in the base course at depths of 127, 279, and 432 mm from the AC surface to measure the vertical stresses. The locations of the gages are summarized in Table 3.

Table 3. Depths of pressure sensors in the test section.

SUBGRADE						
Test window	SUBGRADE			SUBGRADE		
	Longitudinal	Transverse	Vertical	Longitudinal	Transverse	Vertical
707C1	381	381	381			
707C2	381	381	381	686	686	686
707C3	381	381	381			
707C4	381	381	381			
707C5	381	381	381	686	686	686
707C6	381	381	381			

BASE					
Test window	BASE				
	Longitudinal	Transverse	Vertical	Vertical	Vertical
707C2	191	191	191		
707C5	191	191	191		
707C6			127	279	432

For the Dynatest pressure cells the calibration between stress and voltage is

$$\sigma (\text{kPa}) = \frac{(1000 \times V)}{(V_{\text{ex}} \times \text{Gain} \times GF \times 10^{-5})} \quad (1)$$

where σ = measured stress
 V = measured voltage
 V_{ex} = excitation voltage = 10 volts
 GF = gain factor (see table 9)
 Gain = $500 \times \text{A/D card gain} = 1$.

For the Geokon pressure cells the stress conversion from voltage is

$$\sigma (\text{kPa}) = (V \times C) \times 6.895 \quad (2)$$

where σ = measured stress (kPa)
 V = measured voltage (V)
 C = calibration constant.

Moisture Measurements

Soil moisture was measured with Hydra soil moisture probes manufactured by Vitel, Inc. Details on the probe can be found in Janoo et al. (2002). The probe was used to track the in-situ soil moisture and temperature at various depths during accelerated pavement testing.

The Hydra probe also has a built-in thermistor that provides the temperature information needed for the computation of volumetric soil moisture content. The temperature from the thermistor was used as a backup to the thermocouple temperature measurements. The accuracy of thermistor temperatures is $\pm 0.1^\circ\text{C}$.

Nine moisture sensors were installed at three locations at depths of 6, 12, and 24 inches from the top of the AC. We found that the moisture content remained constant during accelerated pavement testing (Table 4).

Table 4. Mean volumetric moisture content (%) for the nine sensors in the test section during accelerated pavement testing. The values in parenthesis are the COV of the mean volumetric moisture content.

Test window	M1	M2	M3	M4	M5	M6	M7	M8	M9
707C1	15.6 (0.6)	21.0 (0.2)	19.4 (0.5)	14.9 (0.5)	21.2 (0.2)	11.7 (0.5)	16.5 (0.6)	12.5 (0.6)	15.6 (0.3)
707C2	15.5 (0.6)	21.0 (0.7)	19.3 (0.7)	14.9 (0.7)	21.3 (0.2)	11.7 (0.5)	16.7 (0.7)	12.5 (1.0)	15.6 (0.6)
707C3	15.5 (0.6)	20.9 (0.9)	19.3 (0.9)	15.1 (0.6)	21.4 (0.3)	11.8 (0.4)	16.9 (0.5)	12.6 (0.9)	15.8 (0.6)
707C4	15.7 (0.5)	21.0 (0.3)	19.4 (0.3)	15.0 (0.5)	21.2 (0.2)	11.7 (0.3)	16.5 (0.7)	12.6 (0.5)	15.7 (0.3)
707C5	15.5 (0.8)	20.9 (0.2)	19.3 (0.4)	14.9 (0.4)	21.2 (0.2)	11.7 (0.4)	16.6 (0.6)	12.5 (0.6)	15.6 (0.4)
707C6	15.5 (0.8)	20.9 (0.9)	19.3 (1.1)	15.1 (0.7)	21.3 (0.3)	11.8 (0.4)	16.8 (0.7)	12.6 (1.2)	15.7 (0.5)

Temperature Measurements

Air, surface, and subsurface temperatures were measured using thermocouple sensors at three locations. These thermocouples have an accuracy of $\pm 0.5^{\circ}\text{C}$. The results again showed that the temperatures were nearly constant during the testing period (Table 5).

Table 5. Mean subsurface temperatures in the test section during accelerated pavement testing.

Test window	Mean temperature (°C)	COV
707C1	19.2	2.0
707C2	19.1	3.8
707C3	20.0	3.2
707C4	19.5	3.2
707C5	18.7	2.8
707C6	19.7	2.6

4 TESTING PROGRAM

Prior to and at the end of the accelerated load tests, FWD measurements were taken on top of the surface of the AC layer at locations shown in Figure 5. Initial transverse profiles were measured using a 3-m-length laser profilometer. The laser, located 45 cm from the ground surface, measures the surface profile at approximately 9-mm intervals. Twenty-four transverse cross-section measurements spaced 0.3 m apart were made in each window. In addition to the profilometer measurements, level surveys were made during every test to determine whether the profilometer reference points moved. The results from the level surveys indicated that the points were stationary throughout the test.

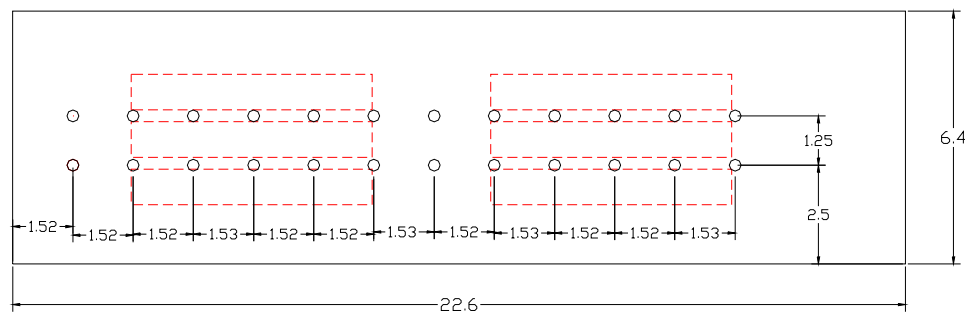


Figure 5. Location of FWD test points in TS 707.

Surface profile measurements were made at or near at 500, 1,000, 2,500, 5,000, 10,000, 25,000, 50,000, 100,000, 200,000, 500,000, 1,000,000, etc. load repetitions. Testing was terminated when a surface rut depth of 12.5 mm was reached or exceeded.

Subsurface stresses, strains, and permanent displacements were also measured in the vertical and two perpendicular horizontal directions at or near 0, 500, 1,000, 2,500, 5,000, 10,000, 25,000, 50,000, 100,000, 200,000, 500,000, 1,000,000, etc. load repetitions. Three repetitions of dynamic stress and strain measurements in the test windows were taken when the wheel was in the middle of the instrumentation (Fig. 6). At the end of the dynamic stress and strain measurements, permanent deformation measurements were taken using the ϵ mu coils. A loose coil gage on the surface was used to measure the permanent deformation between the surface and the first coil in the base course.



Figure 6. Location of test wheels over coil and stress cells.

Accelerated Loading of the Test Sections

The test windows were loaded using the Mark IV Heavy Vehicle Simulator (HVS) accelerated loading system. The tire was a standard dual truck tire set to a pressure of 690 kPa, and the tests were conducted in the uni-directional mode at 13 km/hr. The average number of load repetitions was 700 per hour. The tests were conducted for approximately 22 hours per day, seven days a week. The load was wandered over the test window in 50-mm increments. The mean applied loads are summarized in Table 6.

Table 6. Mean tire loads for each test window.

Test window	Applied load (kN)
707C1	62
707C2	40
707C3	80
707C4	53
707C5	80
707C6	67

Back-calculation of FWD Data

WESDEF (the Corps of Engineers Layered Elastic Evaluation Program) and ELMOD5 were used to back-calculate the layer moduli for TS 707. Twenty-one FWD tests were done on the test section. All tests were adjacent to the test windows. Four drop heights with four repetitions at each drop height were used in the test. No FWD measurements were taken at the end of the test, as the pavement surface was severely deformed.

The deflections were normalized to 40 kN (Table 7), and the Impulse Stiffness Modulus (ISM), which is the ratio of the applied load to the center deflection, was used to select the sites that were within one standard deviation from the mean for backcalculating the layer moduli (Fig. 7). The layer thickness at the selected FWD site was determined from the elevation data and is presented in Table 8.

Table 7. Deflections normalized to 40 kN.

Test number	Deflections (μm) at seven distances (mm) from FWD plate						
	0	305	610	914	1219	1524	1829
1	749	388	124	63	48	37	30
2	634	339	110	51	37	30	24
3	587	309	104	49	36	28	23
4	596	286	91	48	35	28	23
5	538	297	104	45	32	26	22
6	549	293	102	48	34	27	22
7	532	272	94	46	32	24	20
8	701	322	93	47	35	28	24
9	585	313	106	45	32	26	22
10	551	283	91	43	32	25	21
11	628	294	81	39	30	24	20
12	628	306	91	41	31	25	21
13	501	270	99	45	31	25	21
14	686	298	89	42	29	22	18
15	627	306	98	47	34	27	22
16	512	268	95	45	31	25	21
17	498	269	95	45	32	25	21
18	580	281	86	42	31	25	21
19	581	299	96	44	31	25	21
20	502	273	94	43	32	25	21
21	660	297	87	44	30	22	18

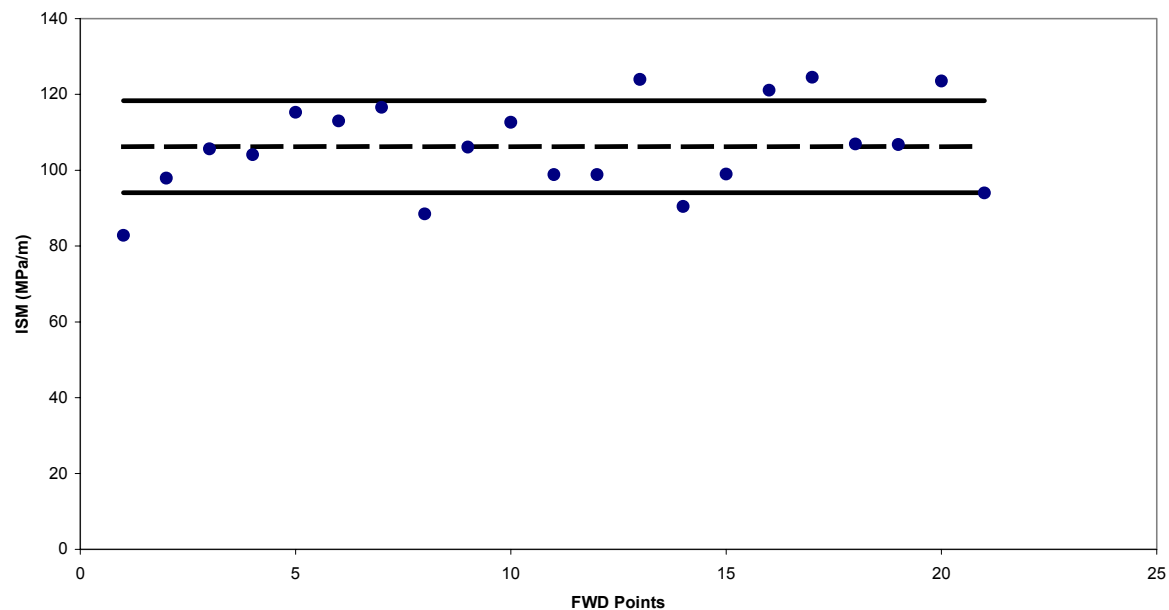


Figure 7. Impulse Stiffness Modulus at FWD test locations.

Table 8. Pavement layer thicknesses used in the back-calculation process.

Location	AC (mm)	Base (mm)	Subgrade (mm)	
			Upper	Lower
2	55	226	1103	2274
3	61	219	1103	2274
4	70	219	1134	2234
5	67	232	1079	2280
6	70	232	1082	2274
7	64	213	1085	2295
9	76	229	1125	2228
10	82	219	1082	2274
11	76	238	1100	2243
12	73	238	1094	2252
15	76	213	1189	2179
18	76	235	1113	2234
19	61	238	1103	2256

We initially tried a four-layer system in WESDEF, using the seed, minimum, maximum, and Poisson's ratios in Table 9. The program also provides an initial seed modulus for the subgrade, based on the outer deflection data. This can be used or reset by the user.

Table 9. Initial and seed moduli used for the various layers.

Material	Modulus (MPa)			Poisson's ratio
	Seed	Min	Max	
AC	2758	3500	20700	0.35
Base	207	7	1030	0.35
Test Subgrade	69	7	165	0.4
Lower Subgrade	69	7	165	0.4

The back-calculated layer moduli are presented in Table 10. The base course modulus was lower than that of the subgrade. We also found that the modulus of the AC layer was high, and we checked the AC modulus based on the frequency of loading, thickness, and temperature. We found that the AC modulus was significantly higher than the back-calculated modulus. We then used the calculated modulus to fix the AC modulus and back-calculated the base and subgrade moduli. We found that, although we doubled the base modulus, the Absolute Arithmetic (AA) error was extremely high (Table 11). We tried several other variations, such as reducing the pavement system to three layers, but were unable to reduce the AA error to an acceptable limit.

Table 10. Back-calculated layer moduli (WESDEF).

Location	Modulus (MPa)				AA (%)
	AC	Base	Upper	Lower	
2	19004	39	316	84	11.8
3	15539	40	346	88	10.0
5	14768	40	407	94	9.6
6	11079	45	341	94	12.7
7	14021	52	287	109	16.2
12	5760	46	352	111	38.2
18	6767	51	350	102	18.4
19	15238	47	327	102	15.0

We tried the radius curvature (Odemark-Boussinesq transformed section approach) method of back-calculation in ELMOD 5. According to Dynatest, “the Radius of Curvature method has been found to agree quite well with the generalized Burmister equations. Comparisons have been made with the CHEVRON, BISTRO and CIRCLY programs, as well as with Finite Element computations. Even for conditions not meeting these limitations, such as layers that are too thin or very non-linear granular materials, the method has been found to provide reasonably correct results. In most of the examples tried, the moduli deviated from the correct values by a factor of less than two.”

Table 11. Back-calculated layer moduli with a fixed AC modulus (WESDEF).

Location	Modulus (MPa)				AA (%)
	AC	Base	Upper	Lower	
2	5972	90	169	97	81.2
3	6040	82	196	99	70.5
5	6141	63	249	97	28.0
6	6968	72	221	108	66.1
7	7000	62	258	99	44.3
12	6935	76	221	114	51.8
18	6173	47	329	104	24.4
19	6040	86	197	115	70.0

The mean back-calculated moduli from ELMOD5 are presented in Table 12.

Table 12. Back-calculated layer moduli (ELMOD5).

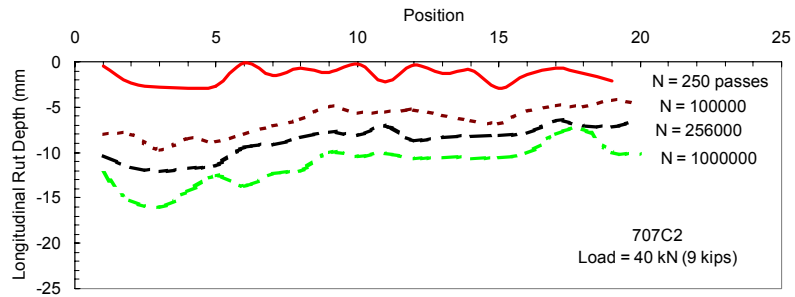
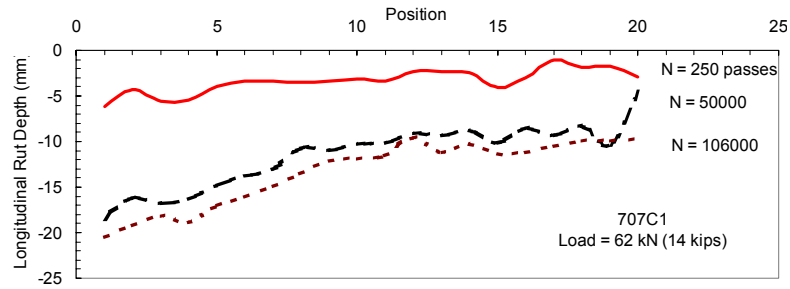
Modulus (MPa)			
AC	Base	Upper	Lower
5603	105	68	58

Surface Rut Measurements

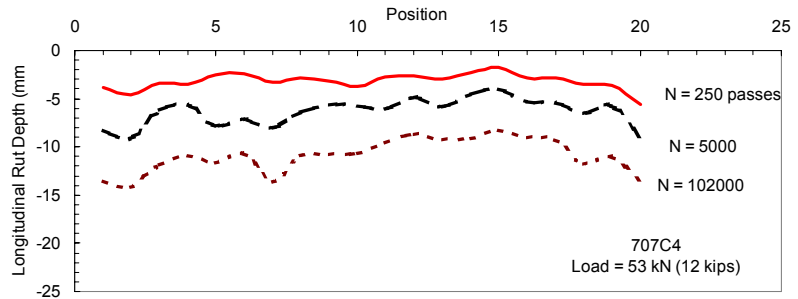
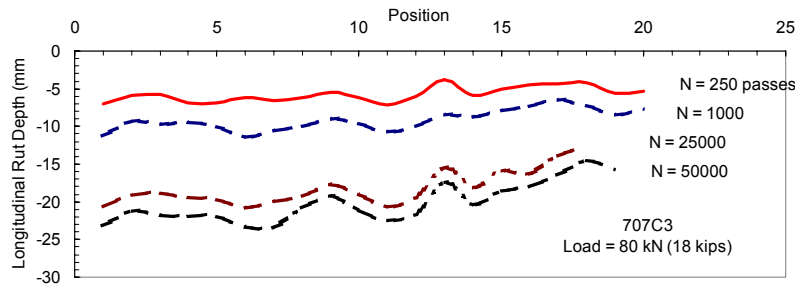
The transverse surface profile was measured periodically during testing. The rut depth was calculated as the difference between the profile measurements taken at the pass level and the profile measurements taken prior to testing. Profile measurements were taken every 305 mm starting from one end of the test window, for a total of 20 locations. These measurements were taken outside the acceleration and deceleration zones

The maximum rut depths from transverse profile measurements were used to develop the longitudinal profile. The longitudinal rut depth in various test windows as a function of load repetitions are presented in Figure 8. As seen in the figure, rutting was fairly uniform throughout the windows, with the exception of 707C1, where there was more rutting on the south side of the test window.

The progression of rut depths as a function of load repetitions in the various windows is presented in Figure 9. In general, as the applied load increased, so did the rate of rut depth.

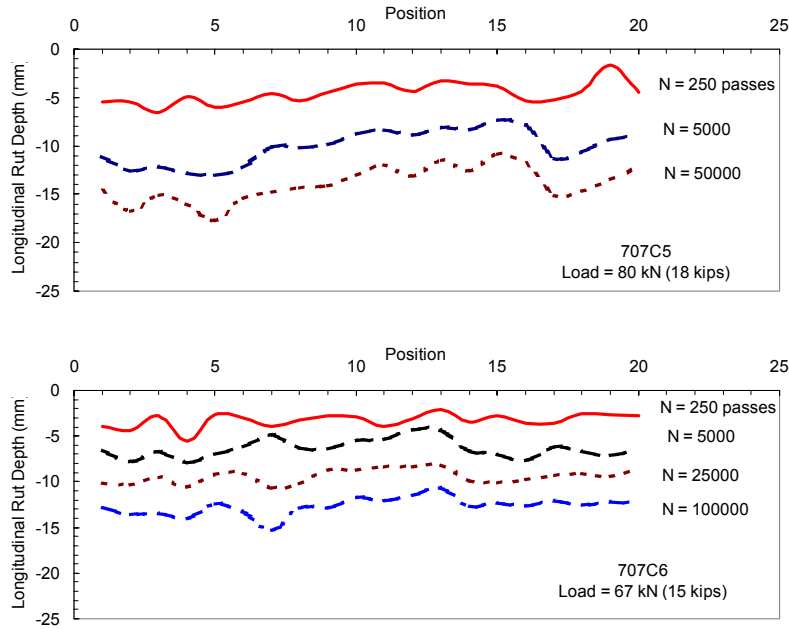


a. TS 707C1 and 707C2



b. TS 707C3 and 707C4.

Figure 8. Longitudinal rut formation as a function of load repetitions.



c. TS 707C5 and 707C6.

Figure 8 (cont.). Longitudinal rut formation as a function of load repetitions.

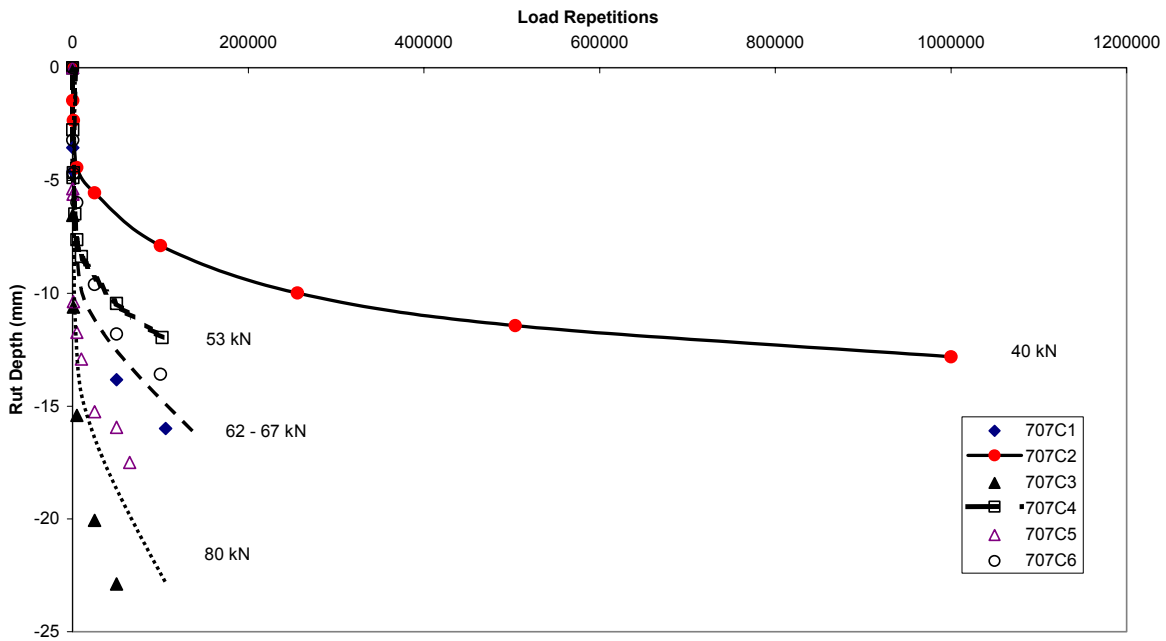


Figure 9. Rut depth progression as a function of load repetitions.

The data from the surface profile measurements were also used to estimate the number of load repetitions required to reach failure. Failure was defined as when the average rut depth reached 12.5 mm. The estimated load repetitions were then used with the appropriate power equations to estimate the failure stresses and strains (Table 13).

Table 13. Load repetitions to reach a failure of 12.5 mm.

Test window	Passes to failure
707C1	35522
707C2	1000000
707C3	2898
707C4	250000
707C5	9444
707C6	71920

Strain Measurements

Permanent Deformations and Strains

Permanent deformation and strain measurements were collected in the base and subgrade. In addition, during the test, a surface coil and the coil under the AC layer were used to determine the deformation of the asphalt layer with increasing load application.

The permanent deformations on the top of the subgrade are shown in Figure 10 as a function of load repetitions. The deformations were compressive, and there is a correlation between applied load and permanent deformation (with the exception of 707C1, which showed non-uniform rutting across the test section).

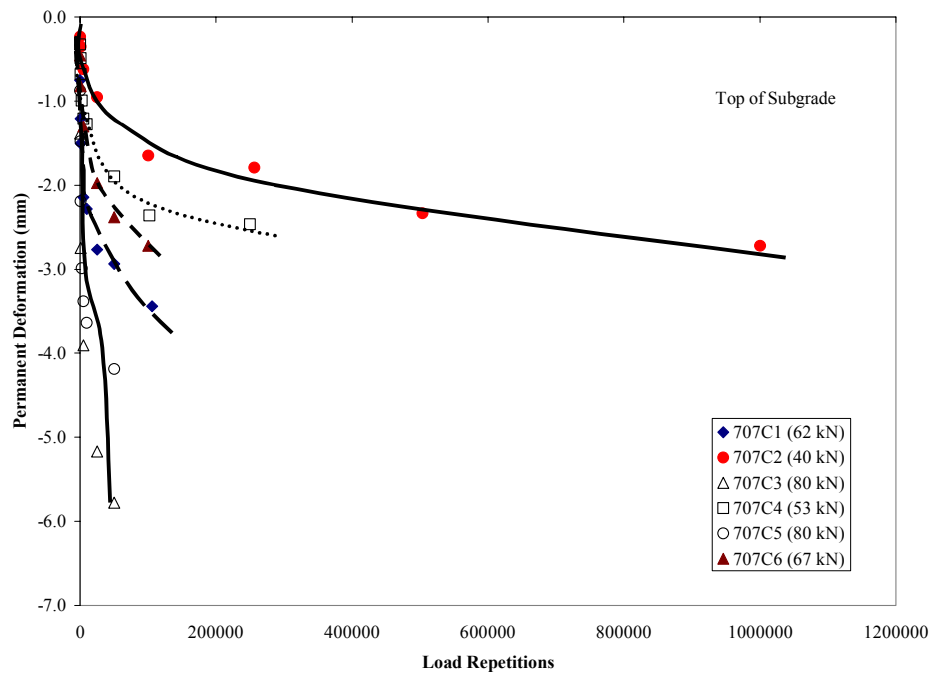


Figure 10. Permanent deformations of the top of the subgrade layer.

The permanent vertical strains in the top of the subgrade as a function of load repetition is presented in Figure 11. Power curves were fitted to the data and the coefficients are presented in Table 14. The permanent strain at the top of the subgrade at failure (12.5 mm surface rut depth) is presented in Figure 12.

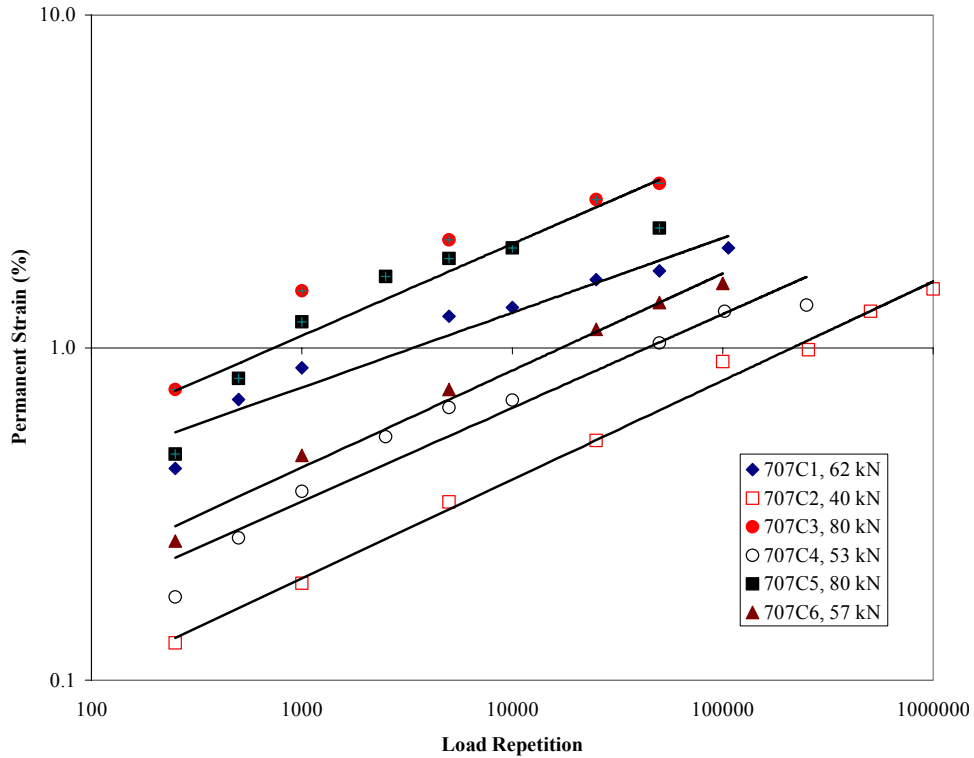


Figure 11. Development of permanent strains on the top of the subgrade as a function of load repetitions.

Table 14. Power curve coefficients for the vertical permanent strains.

Test window	Load (kN)	A	n	R ²
707C1	62	0.1610	0.2245	0.94
707C2	40	0.0259	0.2977	0.99
707C3	80	0.1614	0.276	0.86
707C4	53	0.0491	0.2818	0.95
707C5	80	0.1614	0.276	0.86
707C6	67	0.0581	0.2918	0.99

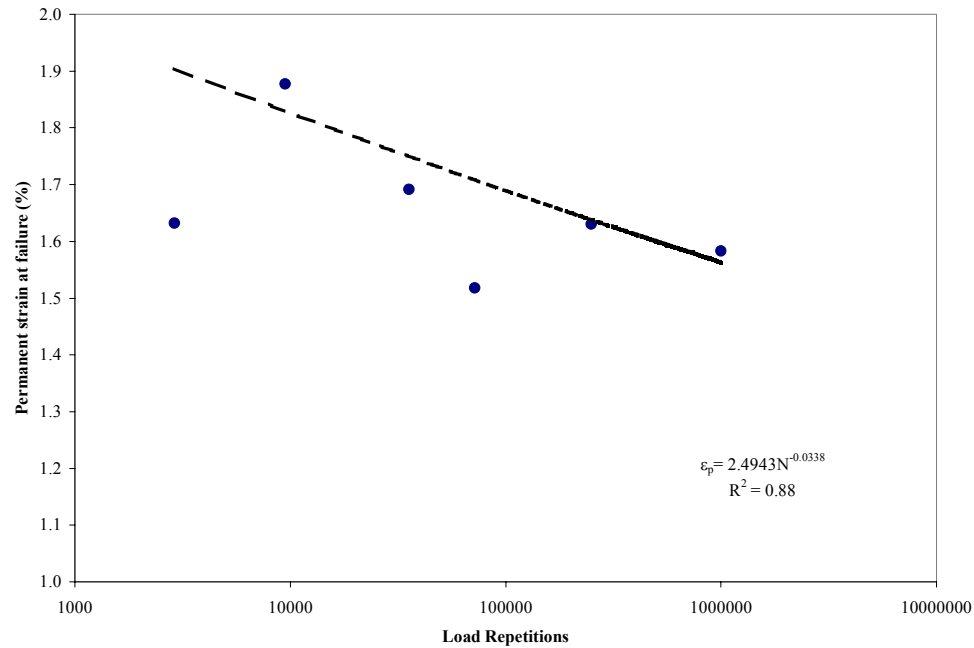


Figure 12. Permanent deformations at failure on the top of the subgrade.

Dynamic Displacements and Strains

As with previous test sections, triaxial dynamic displacements were measured with the ϵ mu coil gages in the base and subgrade. The vertical displacements were compressive, whereas the peak longitudinal and transverse displacements were tensile. The peak displacements were used to calculate the peak strains. The peak vertical displacements (strains) were compressive. The change in the vertical displacement as a function of load repetitions at the top of the subgrade is shown in Figure 13.

The change in vertical strain as a function of load repetition is presented in Figure 14. Power curves were fitted to the data. The power curve coefficients are presented in Table 15.

The measured strains were corrected for speed, and the following equation can be used to predict the dynamic strain for this subgrade:

$$\epsilon_e = 0.0064 N^{-0.1769} \quad R^2 = 0.90 \quad (3)$$

where ϵ_e is dynamic strain and N is the number of load repetitions.

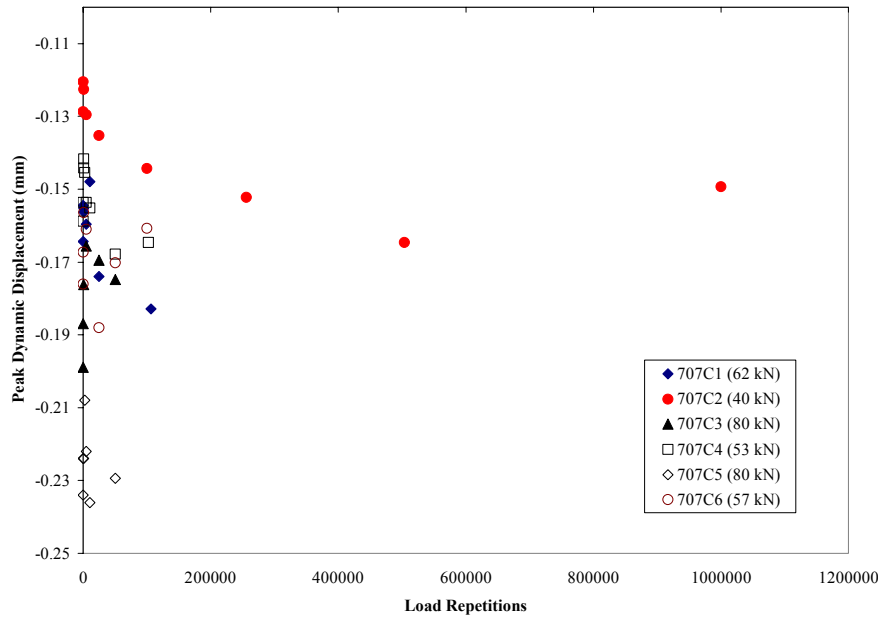


Figure 13. Peak dynamic vertical displacements at the top of the subgrade as a function of load repetitions.

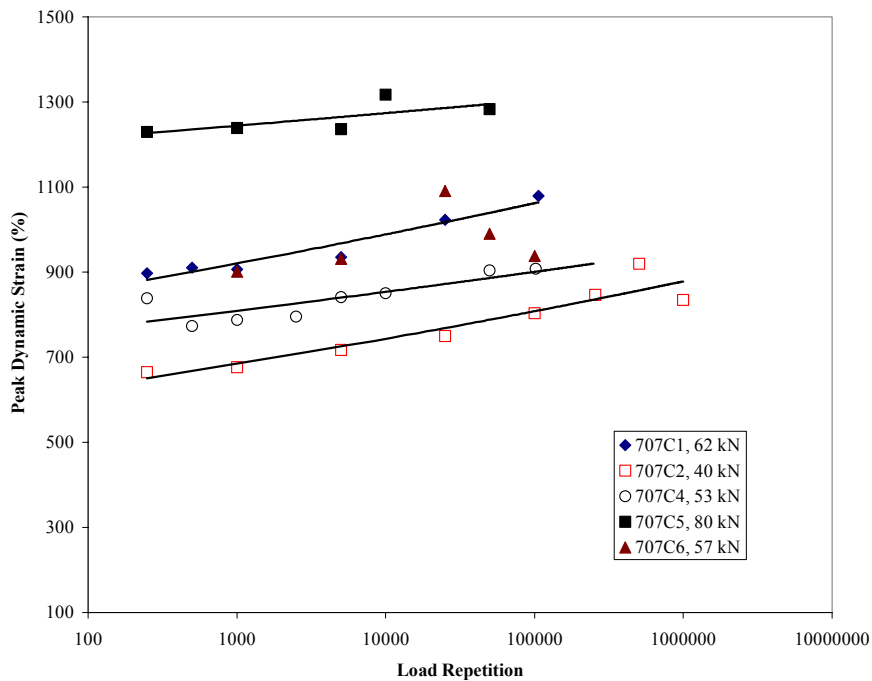


Figure 14. Peak dynamic vertical strains of the subgrade as a function of load repetitions.

Table 15. Power curve coefficients for the vertical strains.

Test window	Load (kN)	A	n	R ²
707C1	62	742.57	0.0311	0.93
707C2	40	532.83	0.0362	0.9
707C3	80			
707C4	53	688.85	0.0233	0.68
707C5	80	1159	0.0102	0.5
707C6	57	742.57	0.0311	0.93

Stress Measurements

Vertical, longitudinal, and transverse stress measurements were made at 76 mm from the top of the subgrade. In 707C2 and 707C5, additional measurements were made at a depth of 381 mm from the top of the subgrade. The measured stresses were compressive, and the peak values are presented in Table 16.

Table 16. Peak stresses in the top of the subgrade under applied load.

Test window	Load (kN)	Depth from top of AC (mm)	Stress (kPa)			
			Repetition	Vertical	Longitudinal	Transverse
707C1	62	381	0	135.59	20.72	20.37
			250	128.35	20.72	20.36
			500	127.37	20.59	20.49
			1000	125.41	20.62	20.53
			5000	130.76	21.80	21.08
			10000	127.94	21.51	20.81
			25000	139.69	23.54	22.33
			50000	133.79	23.07	21.78
			106000	146.74	25.08	23.43
707C2	40	381	0	74.89	17.37	10.96
			250	71.43	16.86	10.76
			1000	72.74	18.05	11.46
			5000	72.97	18.87	11.92
			25000	76.43	21.71	12.53
			100000	83.60	24.78	13.02
			256000	85.21	24.96	13.45
			504000	91.46	27.23	14.33
			1000000	86.67	26.09	13.93

Table 16 (cont.). Peak stresses in the top of the subgrade under applied load.

Test window	Load (kN)	Depth from top of AC (mm)	Stress (kPa)			
			Repetition	Vertical	Longitudinal	Transverse
707C2	40	686	0	12.36	25.96	2.99
			250	12.66	24.90	2.90
			1000	12.82	26.70	3.25
			5000	13.01	27.26	3.70
			25000	13.78	30.71	3.91
			100000	14.69	32.66	4.63
			256000	16.61	34.57	5.04
			504000	17.10	38.15	5.22
			1000000	16.21	36.98	5.02
707C3	80	381	0	111.06	22.02	27.22
			250	108.69	21.04	25.95
			1000	109.96	21.22	25.88
			5000	111.43	21.43	25.38
			25000	122.49	22.55	26.36
			50000	126.90	22.26	26.37
707C4	53	381	0	126.21	21.34	18.83
			250	117.92	21.03	18.62
			500	114.20	20.78	18.15
			1000	113.27	21.37	18.00
			2500	111.57	21.31	17.89
			5000	120.10	22.34	19.22
			10000	119.61	22.64	19.52
			50000	122.02	22.62	21.18
			250000	114.02	21.53	20.97
707C5	80	381	0	105.86	23.63	18.19
			250	105.97	22.72	17.77
			500	106.42	22.51	17.24
			1000	109.80	22.36	17.29
			2500	111.41	20.93	16.85
			5000	120.25	22.59	18.32
			10000	122.64	23.27	18.51
			50000	125.63	23.99	18.48

Table 16 (cont.). Peak stresses in the top of the subgrade under applied load.

Test window	Load (kN)	Depth from top of AC (mm)	Stress (kPa)			
			Repetition	Vertical	Longitudinal	Transverse
707C5	80	686	0			7.11
			250			6.82
			500			6.42
			1000			6.38
			2500			6.44
			5000			7.37
			10000			8.19
			50000			8.09
707C6	67	381	0	120.27	17.96	17.07
			250	112.85	16.76	14.93
			1000	111.32	16.18	14.06
			5000	109.59	15.77	13.68
			25000	126.02	18.48	15.75
			50000	113.60	18.01	14.68
			100000	112.14	18.35	14.59

The measured vertical stresses were compared with the predicted stresses using the back-calculated moduli from the FWD measurements. The results are presented in Figure 15.

The results indicate that the stresses calculated from the back-calculated moduli from ELMOD and WESDEF (fixed AC) were closer to the measured values. The exception is at a load of 80 kN, where the measured stresses decrease, indicating a non-linear material modulus. It is also interesting that the moduli from WESDEF with the fixed AC modulus did better in predicting the stresses than the solution from WESDEF where the AC layer was also back-calculated. The error between the measured and calculated deflections with the fixed AC was significantly higher. Does this suggest that getting a good fit between measured and calculated deflections is not as critical as one thinks?

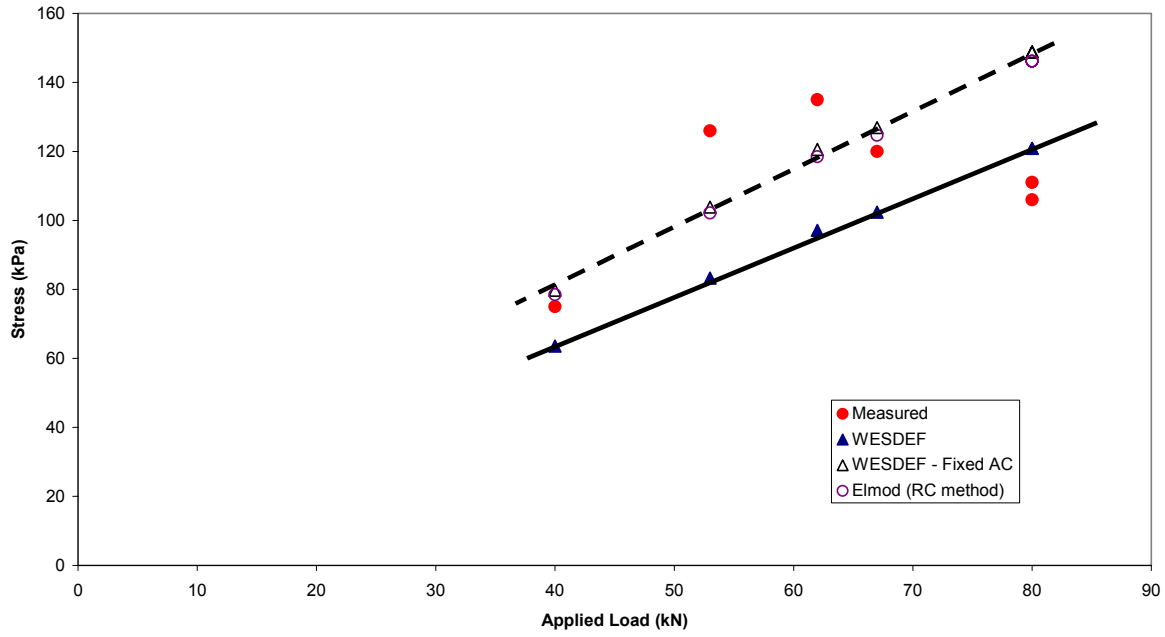


Figure 15. Comparison of calculated and measured stresses.

5 FORENSICS

TS 707 was built with an AASHTO A-2-4 subgrade soil conditioned to 12% gravimetric moisture content. The optimum moisture content for this soil is 9%. The actual mean subgrade soil gravimetric moisture content during construction was 12.0%. The mean subgrade soil gravimetric density measured during the forensic exploration was 11.0%. Therefore, 1% of moisture was lost to the environment during the period of the accelerated traffic tests (Fig. 16).

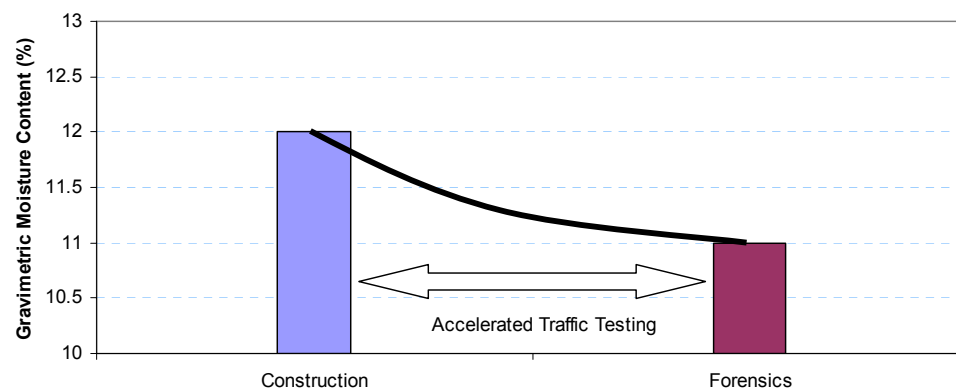


Figure 16. Subgrade mean gravimetric moisture content from the time of construction to the time of the forensic evaluation.

At the end of the traffic tests the pavement surface had smooth rut profiles in the test windows. No cracking or other surface deterioration was detected.

Forensic Testing

A trench was excavated across test windows 1, 2, and 3 on the south region of the test section (Fig. 17). Another trench was excavated in the north region of the test section, cutting across test windows 4, 5, and 6.

The locations of the forensic trenches were chosen carefully to avoid damaging the embedded sensors. The boundaries of the trenches were marked with paint over the asphalt pavement and then cut with a diamond saw without adding water (Fig. 18). Dry saw cutting increases wear on the blade, but it was necessary to avoid altering the moisture content of the soils in the trenches. Saw cutting produced neat trench sides so that reliable layer thickness measurements could be made.

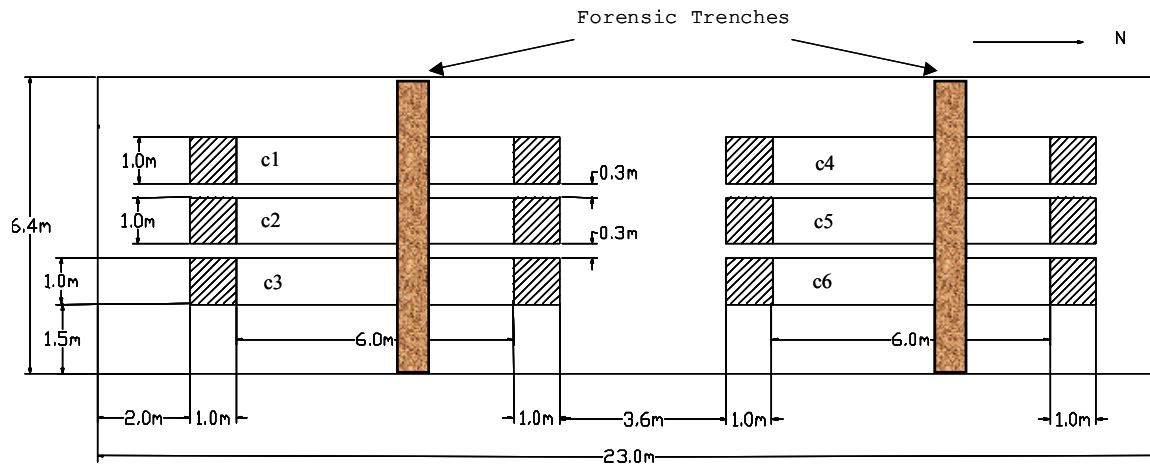
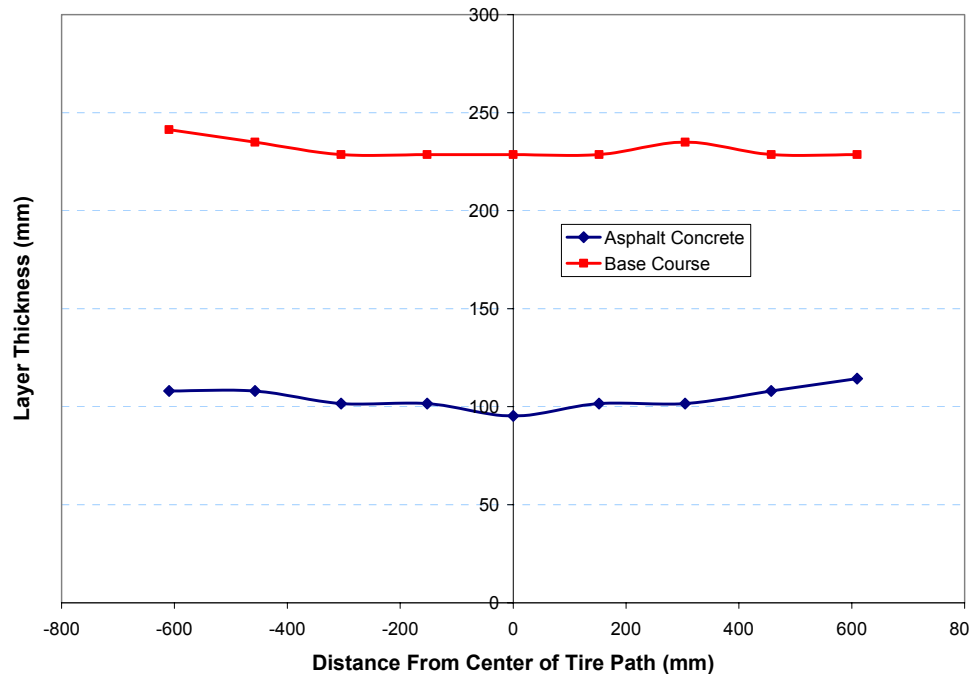


Figure 17. Location of the forensic trenches in TS 707.

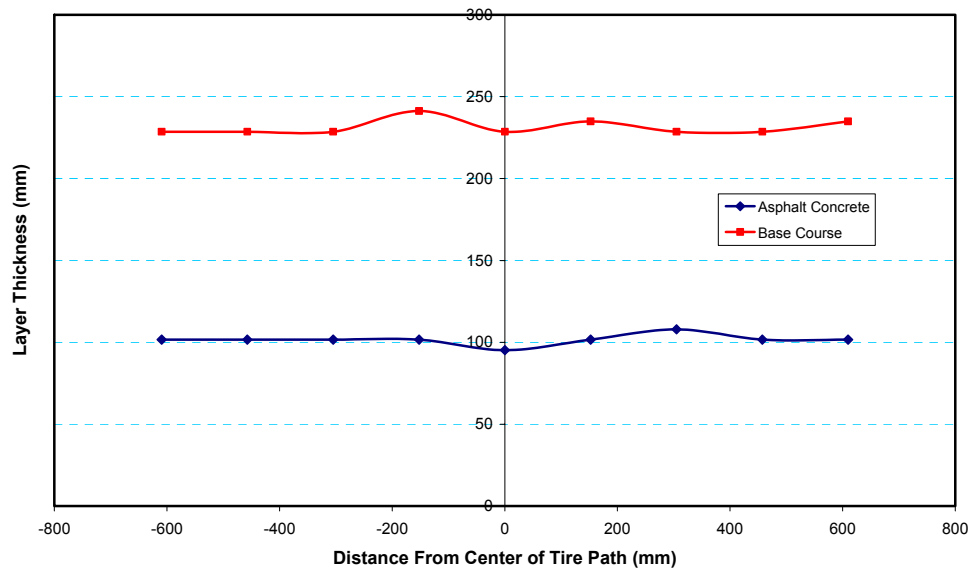


Figure 18. Dry saw cutting of the asphalt layer.

Asphalt concrete and base course layer thickness measurements were taken at the center of each test window and at 0.15, 0.30, 0.45, and 0.60 m to the right and to the left from the center. The results are shown in Figure 19.

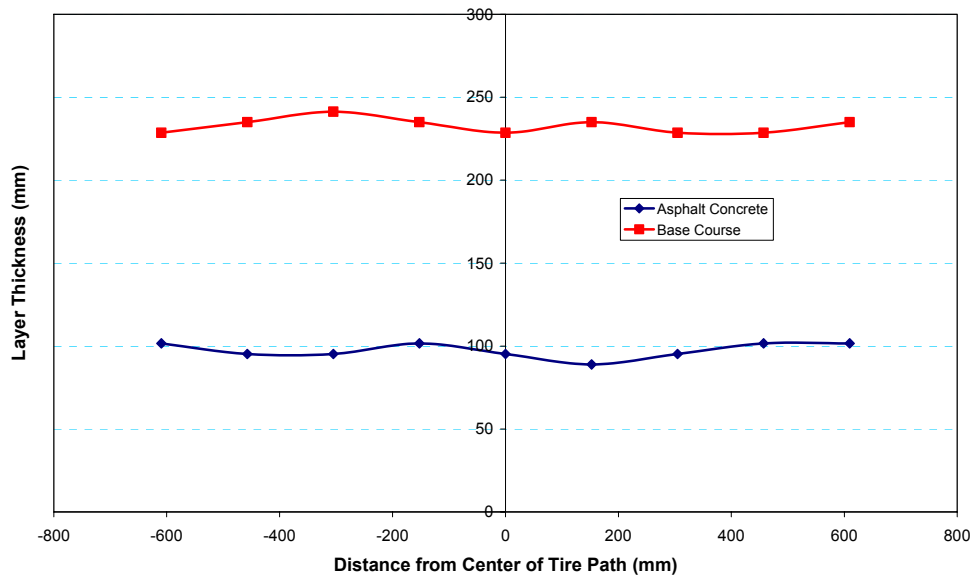


a. Test Window c1.

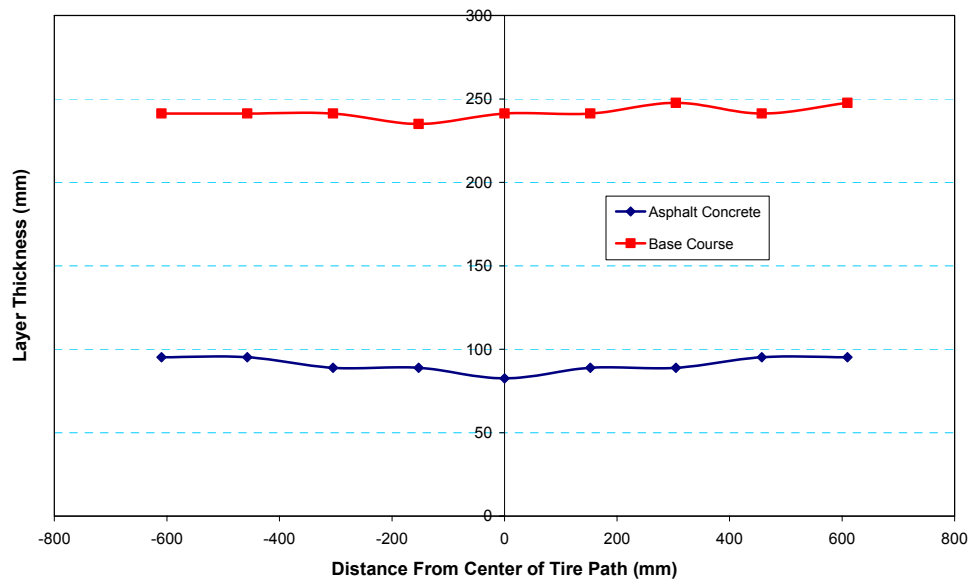


b. Test Window c2.

Figure 19. Thickness measurements in the asphalt concrete layer and in the base course in cross sections of the six test windows.

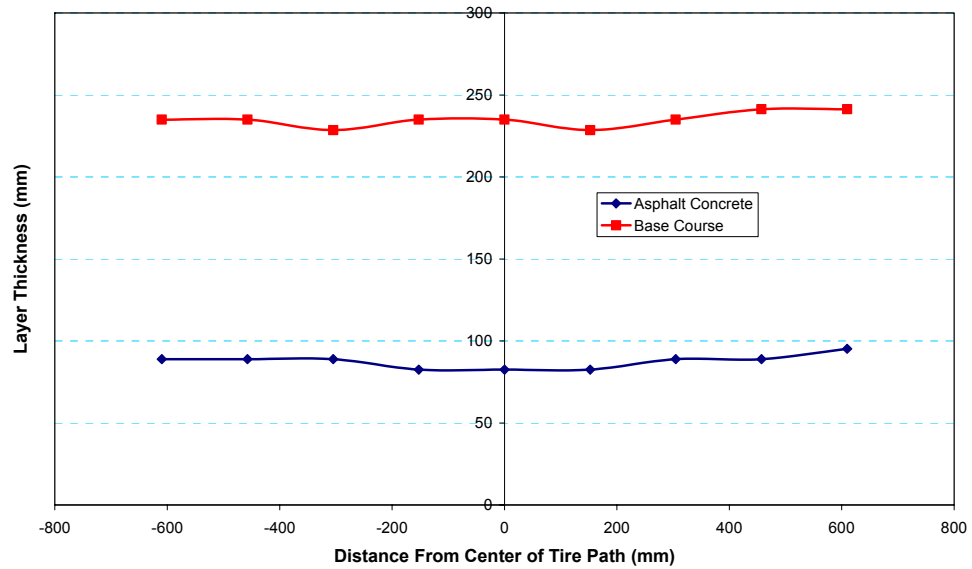


c. Test Window c3.

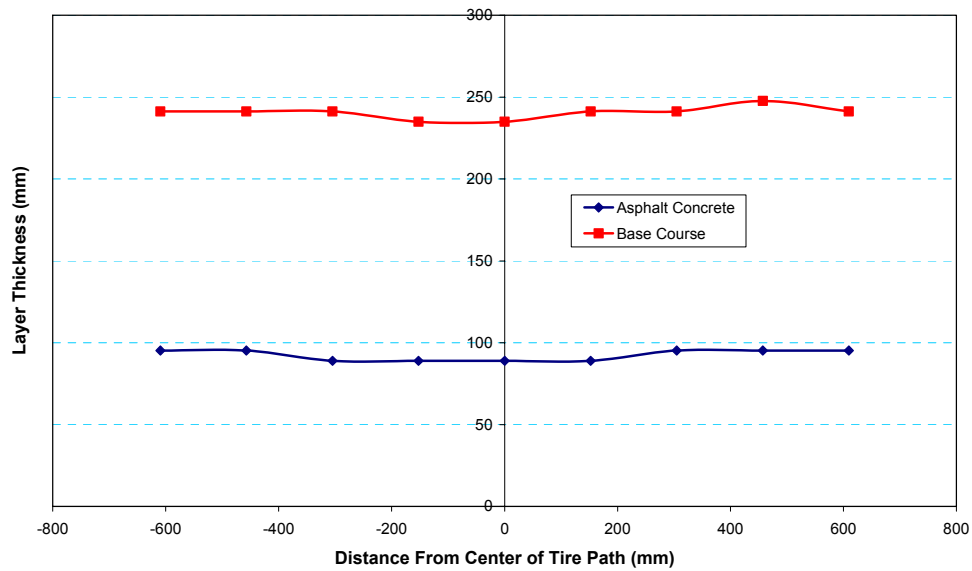


d. Test Window c4.

Figure 19 (cont.). Thickness measurements in the asphalt concrete layer and in the base course in cross sections of the six test windows.



e. Test Window c5.



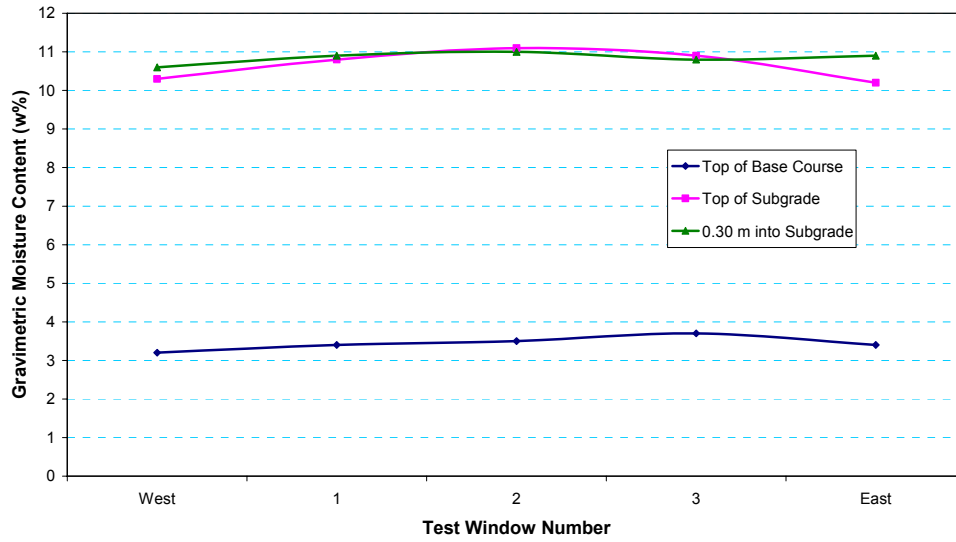
f. Test Window c6.

Figure 19 (cont.). Thickness measurements in the asphalt concrete layer and in the base course in cross sections of the six test windows.

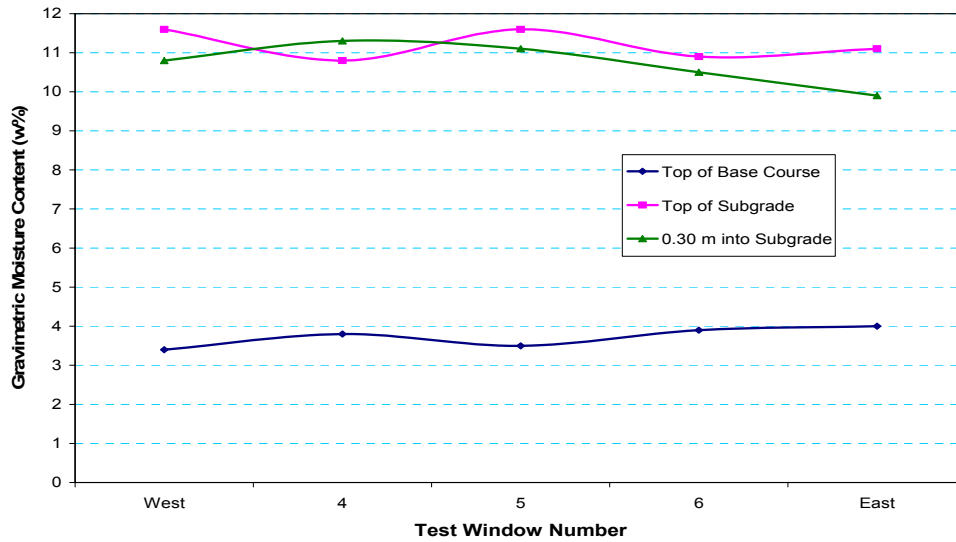
As soon as the asphalt layer was removed from the trenches, nuclear moisture and density measurements were conducted by means of a Troxler gage (Fig. 20). The test locations in the trenches were chosen to represent the center of each test window and areas outside the test windows on the east and west sides. The measurements were conducted with the probe inserted 15 cm into the soil. The measurement represents the region of soil between the inserted nuclear source and the receiver in the box of the apparatus. The gravimetric moisture contents are shown in Figure 21. The soil dry densities are shown in Figure 22.



Figure 20. Nuclear gage density measurements in the trenches.

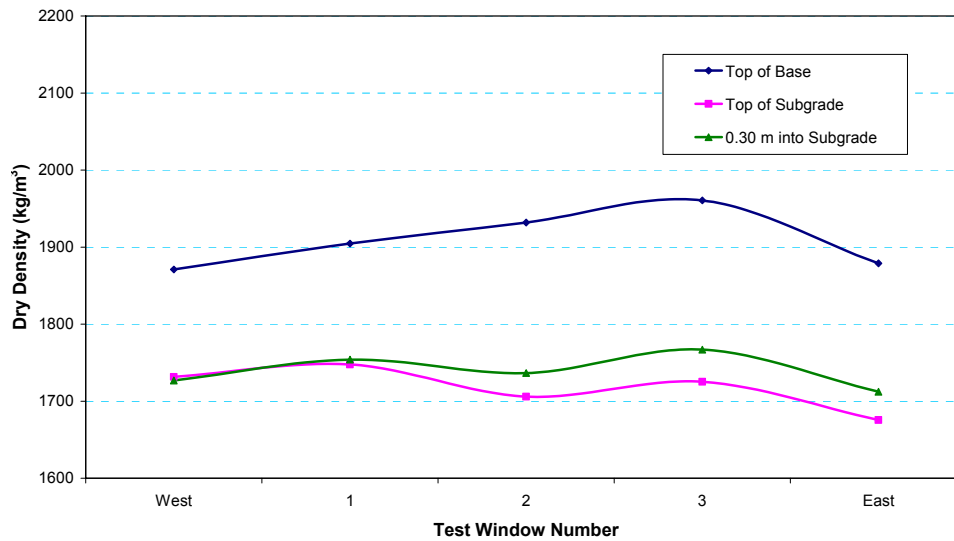


a. South trench.

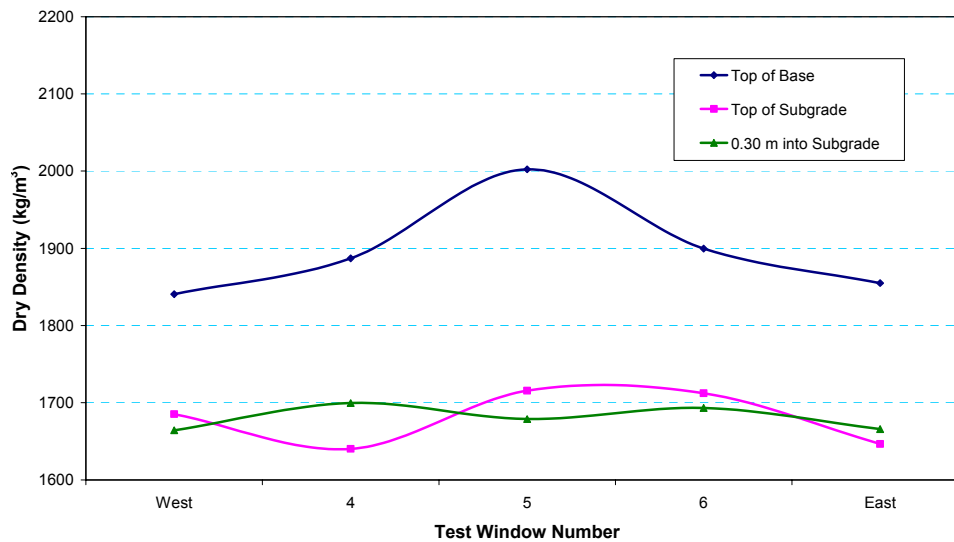


b. North trench.

Figure 21. Gravimetric moisture content in the two forensic trenches obtained with a nuclear gage.



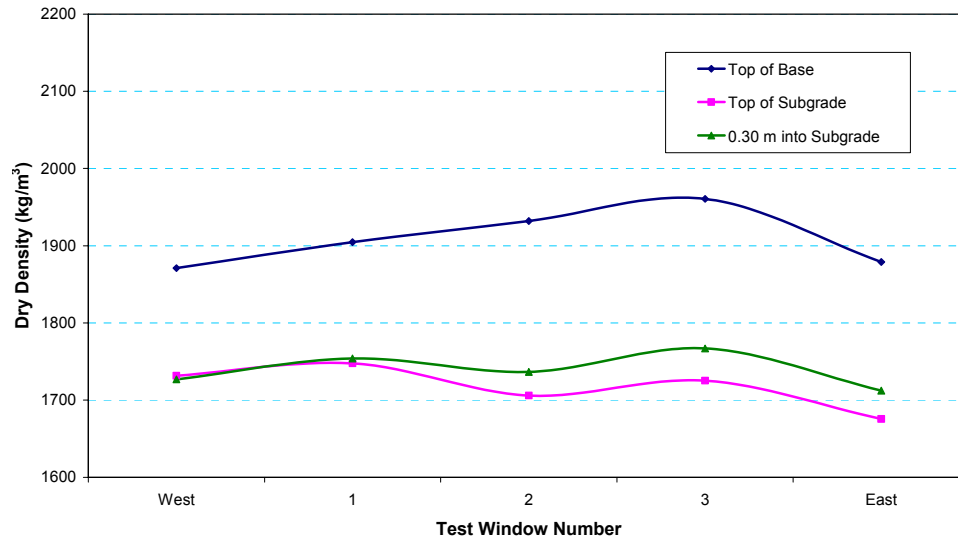
a. South trench.



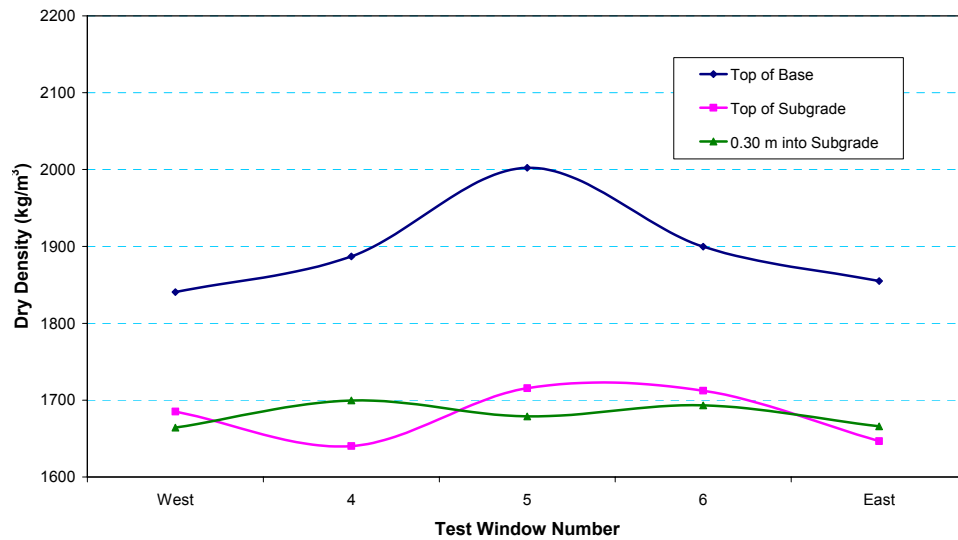
b. North trench.

Figure 22. Soil dry density in the two forensic trenches obtained with a nuclear gage.

Sand cone measurements were conducted at the same locations where the nuclear gage measurements were taken (Fig. 23). This allows direct comparison of the test results obtained with the two methods.



a. South trench.



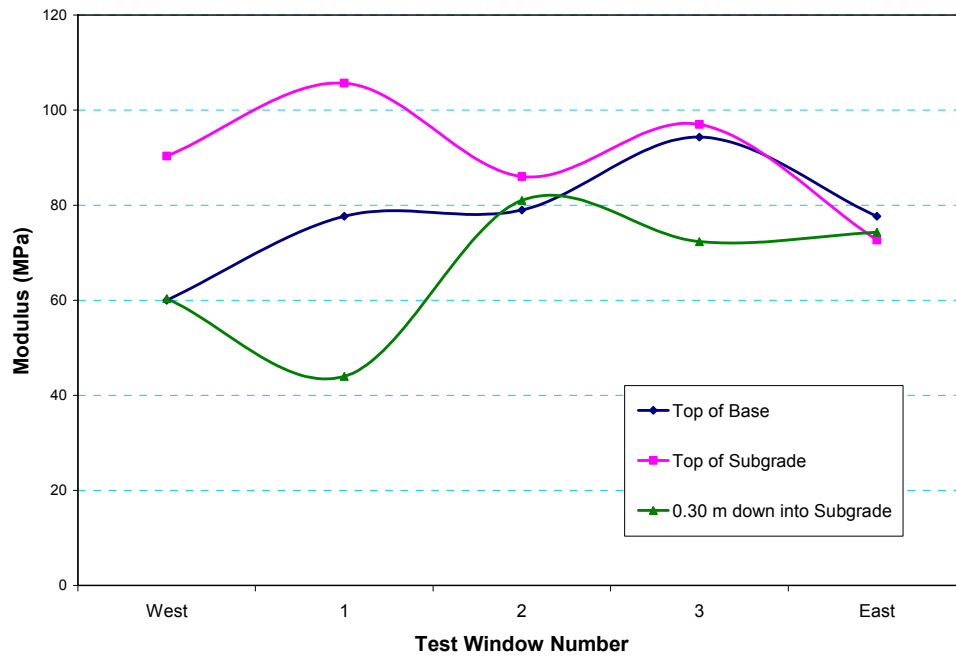
b. North trench.

Figure 23. Soil dry density in the two forensic trenches obtained with a sand cone.

A portable falling weight deflectometer was used to measure the composite soil modulus at various layers in the subgrade at the trenches (Fig. 24). The results are presented in Figure 25.

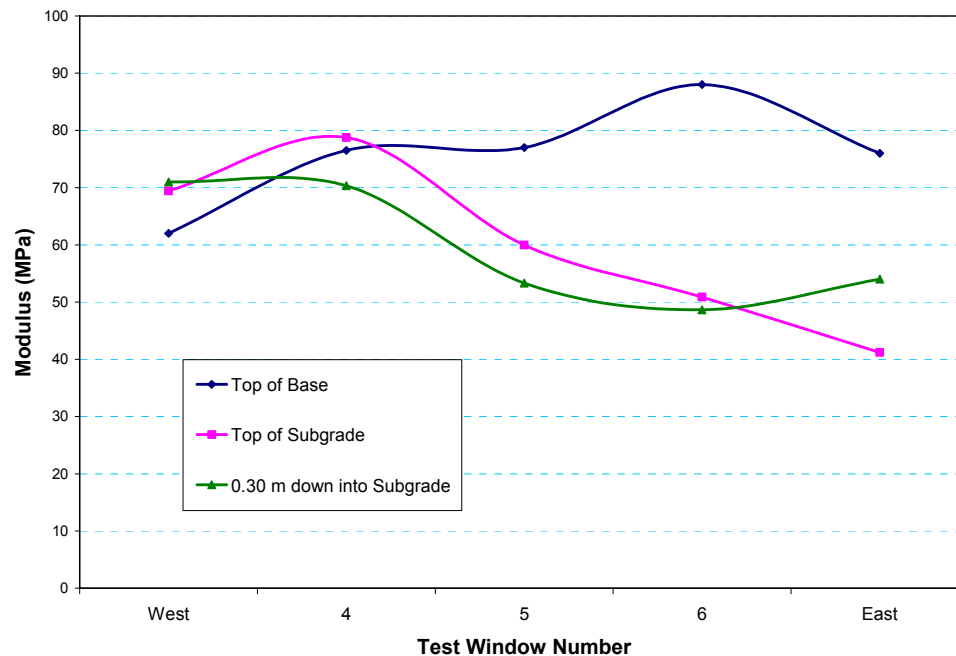


Figure 24. Portable falling weight deflectometer being used in the trenches.



a. South trench.

Figure 25. Soil modulus as measured with the portable falling weight deflectometer in the two forensic trenches.



b. North trench.

Figure 25 (cont.). Soil modulus as measured with the portable falling weight deflectometer in the two forensic trenches.

Dynamic cone penetrometer (DCP) measurements were conducted in the trenches at each test window in the traffic area and at each side of the trenches outside the traffic area (Fig. 26). DCP tests were initiated on the top of the subgrade and at depths of 0.30 and 0.60 m in the subgrade. The DCP measurements were correlated to California Bearing Ratio (CBR) values using the equation

$$\text{Log CBR} = 2.46 - 1.12 \times \log \text{DCP} \quad (4)$$

where DCP is in mm per blow. The results are shown in Figure 27.

This correlation was developed at the Army Corps of Engineers Waterways Experiment Station (WES) (Webster et al. 1992). WES developed the above correlation based on testing of a variety of soils. The DCP test apparatus used at CRREL was manufactured by Kessler Soils Engineering Products, Inc. (<http://www.kesslerdcp.com/info.html>). The DCP–CBR conversions were obtained using an automated Excel spreadsheet provided by the instrument manufacturer. The spreadsheet implements the CBR–DCP correlations developed by WES.

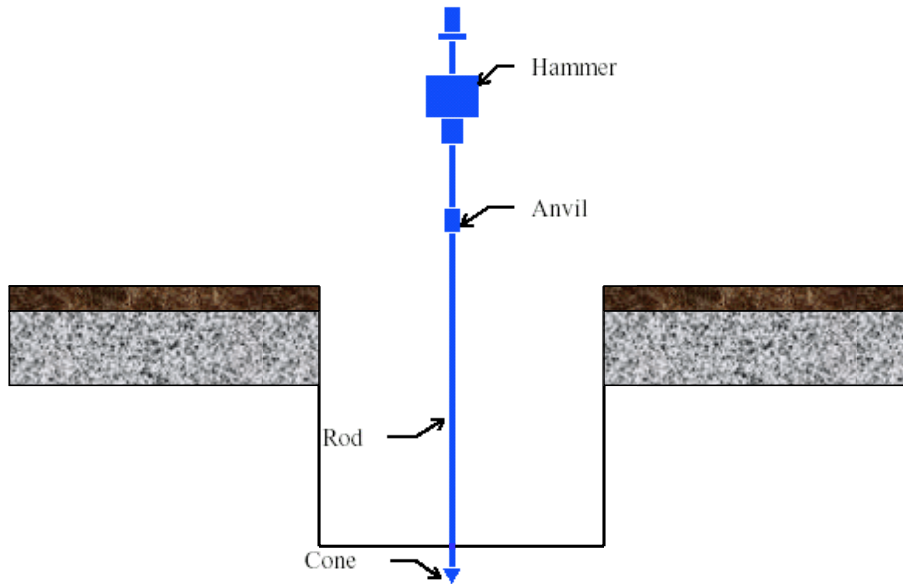
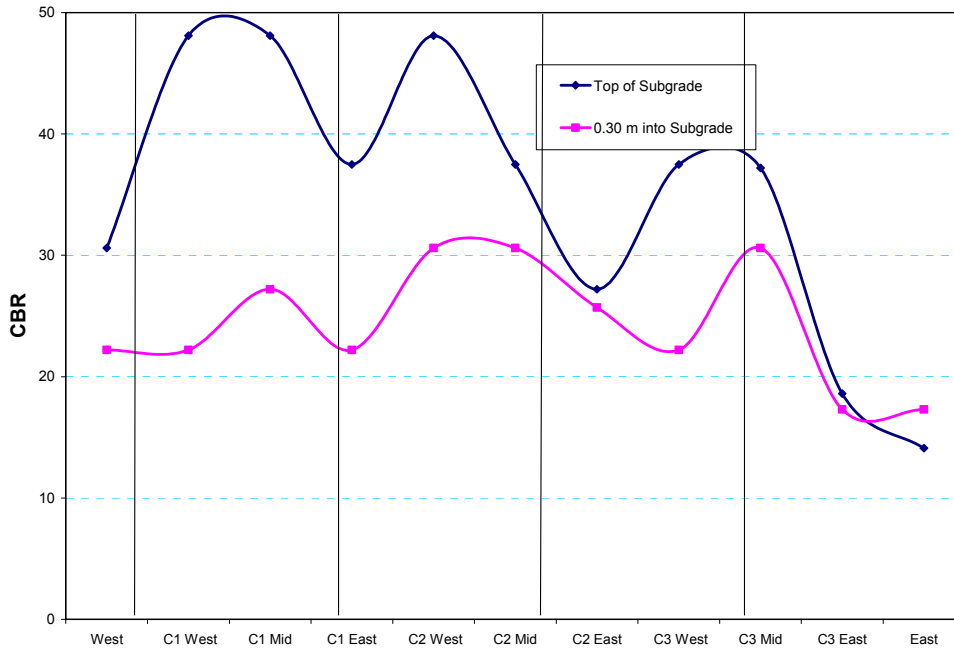
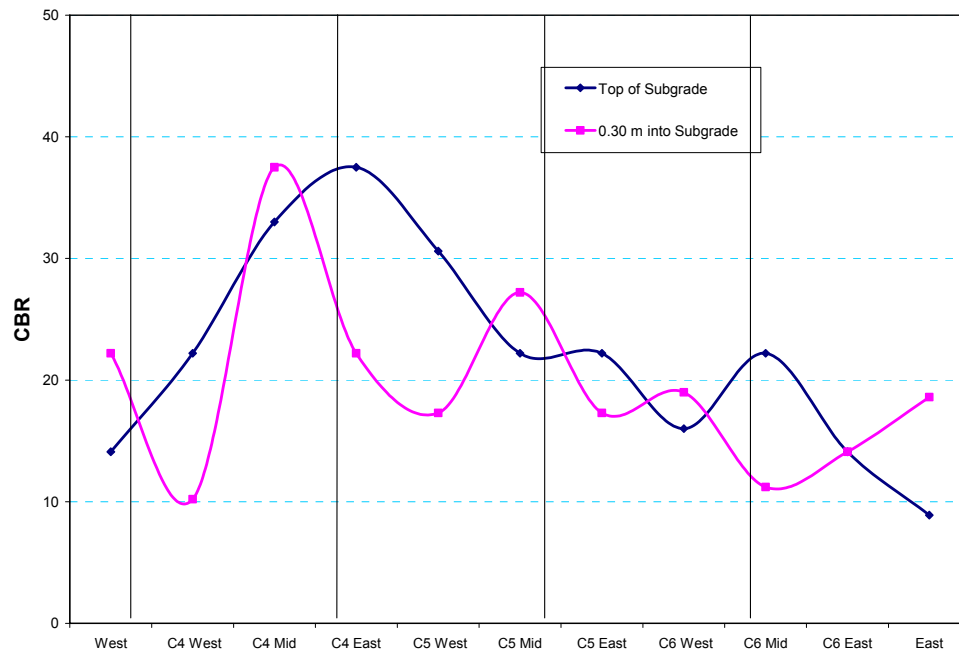


Figure 26. Dynamic cone penetrometer.



a. South trench.

Figure 27. CBR values obtained from DCP measurements in the two forensic trenches.



b. North trench.

Figure 27 (cont.). CBR values obtained from DCP measurements in the two forensic trenches.

Forensic Observations

At the end of traffic loading the surface ruts in the test windows of this test section were smooth and of the expected shape for wandered traffic. No crack was detected in the test windows.

The moisture content in the upper subgrade gradually changed from 12% during construction to 11% by the time of the forensic evaluation. This is not surprising for an AASHTO soil type A-2-4. This loss may be the result of some diffusion through the base course and the asphalt concrete.

The subgrade soil contained a significant number of gravel-size particles. Vane shear tests and drive cylinder tests were not conducted because the gravel particles prevented proper sampling.

The asphalt concrete thickness was designed to be 76 mm, but the actual average thickness was 96 mm. The average thickness of the base course layer was 236 mm compared to a design thickness of 229 mm.

Except for the asphalt concrete thickness, no significant anomaly was found during the forensic examination.

6 SUMMARY AND CONCLUSIONS

Accelerated pavement testing was conducted on a test section with an A-2-4 subgrade soil placed at slightly wetter than the optimum density and moisture content (1930 kg/m³ and 12%, respectively). The subgrade layer was instrumented with stress, strain, temperature, and moisture sensors.

The test section was divided into six test windows, and accelerated pavement testing was conducted over a period of 11 months. During the accelerated testing, dynamic stresses, dynamic and permanent strains, and surface rut depth measurements were collected at given loading intervals. Stress measurements were collected in all of the six test windows. Strain measurements were collected in all six windows to a depth of 1.2 m into the subgrade. Stress and strain measurements were made in the vertical, longitudinal, and transverse directions of loading. Temperature and moisture measurements were made every 4 hours during the tests. The test loads varied between 40 and 80 kN. The average tire pressure was 690 kPa.

The dynamic strains at failure are compared with the current Asphalt Institute and Shell subgrade failure criteria in Figure 28. In addition the strains at failure from the other subgrades are shown in Figure 28.

In terms of predicting the allowable number of load repetitions, N_d , to limit rutting on top of the subgrade, the following equation was used:

$$N_d = f_4 (\varepsilon_v)^{-f_5} \quad (4)$$

where the coefficients f_4 and f_5 are 0.0064 and -0.1769 , respectively, for the A-2-4 soil at a moisture content of 12%.

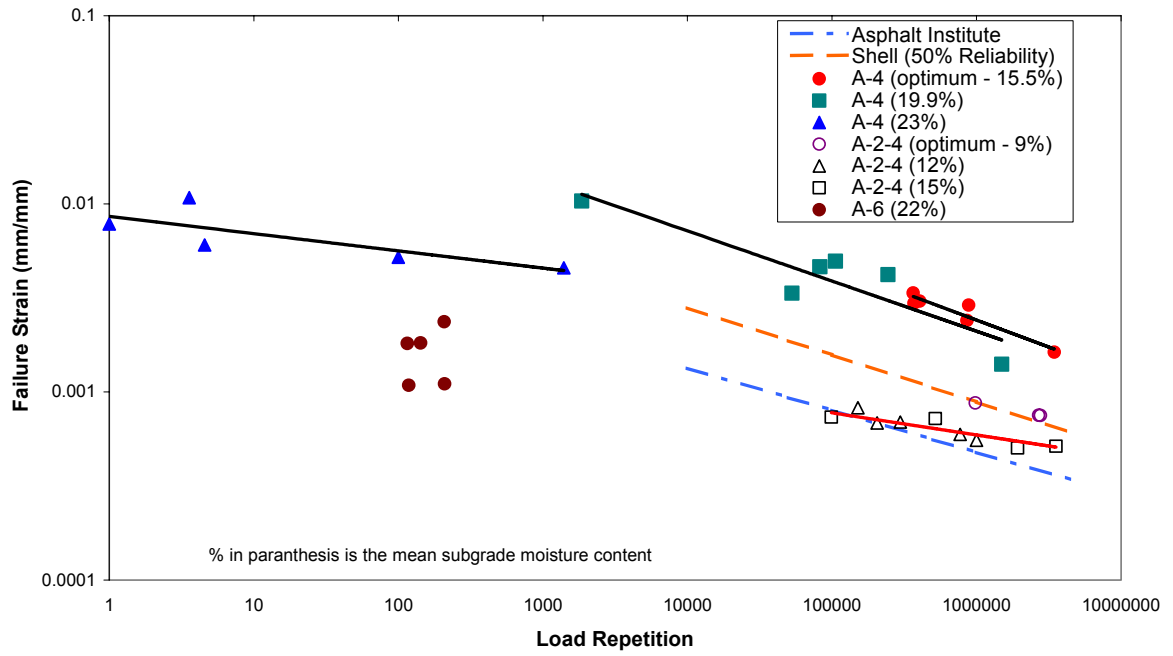


Figure 28. Effect of soil type on the subgrade failure criterion.

REFERENCES

Janoo, V., L. Irwin, and R. Haehnel (2002) Pavement subgrade performance study: Project overview. Technical Report ERDC/CRREL TR-03-5, Engineer Research and Development Center, Cold Regions Research and Engineering Laboratory, Hanover, New Hampshire.

Webster, S.L., R.H. Grau, and T.P. Williams (1992) Description and application of dual mass dynamic cone penetrometer. Instruction Report GL-92-3, U.S. Army Waterways Experiment Station, Vicksburg, Mississippi.